Huntingtin Aggregation Kinetics and Their Pathological Role in a *Drosophila* Huntington's Disease Model

Kurt R. Weiss,* Yoko Kimura,*,† Wyan-Ching Mimi Lee,* and J. Troy Littleton*,[1]

*The Picower Institute for Learning and Memory, Department of Biology and Department of Brain and Cognitive Sciences, Massachusetts Institute of Technology, Cambridge, Massachusetts 02139, and †Laboratory of Protein Metabolism, The Tokyo Metropolitan Institute of Medical Science, Kamikitazawa, Setagaya-Ku, Tokyo 156-8506, Japan

ABSTRACT Huntington's disease is a neurodegenerative disorder resulting from expansion of a polyglutamine tract in the Huntingtin protein. Mutant Huntingtin forms intracellular aggregates within neurons, although it is unclear whether aggregates or more soluble forms of the protein represent the pathogenic species. To examine the link between aggregation and neurodegeneration, we generated *Drosophila melanogaster* transgenic strains expressing fluorescently tagged human *huntingtin* encoding pathogenic (Q138) or nonpathogenic (Q15) proteins, allowing *in vivo* imaging of Huntingtin expression and aggregation in live animals. Neuronal expression of pathogenic Huntingtin leads to pharate adult lethality, accompanied by formation of large aggregates within the cytoplasm of neuronal cell bodies and neurites. Live imaging and Fluorescence Recovery After Photobleaching (FRAP) analysis of pathogenic Huntingtin demonstrated that new aggregates can form in neurons within 12 hr, while preexisting aggregates rapidly accumulate new Huntingtin protein within minutes. To examine the role of aggregates in pathology, we conducted haplo-insufficiency suppressor screens for Huntingtin-Q138 aggregation or Huntingtin-Q138–induced lethality, using deficiencies covering ~80% of the *Drosophila* genome. We identified two classes of interacting suppressors in our screen: those that rescue viability while decreasing Huntingtin expression and aggregation and those that rescue viability without disrupting Huntingtin aggregation. The most robust suppressors reduced both soluble and aggregated Huntingtin levels, suggesting toxicity is likely to be associated with both forms of the mutant protein in Huntington's disease.

HUNTINGTON'S disease (HD) is an autosomal dominant neurodegenerative disorder and one of the first characterized members of a family of neurological diseases that result from expansion of a polyglutamine [poly(Q)] tract within the causative protein (Orr and Zoghbi 2007). HD is characterized by neurodegeneration and formation of neuronal intracellular inclusions, primarily in the striatum and cortex, leading to motor impairment, personality disorders, dementia, and ultimately death (Vonsattel *et al.* 1985; Portera-Cailliau *et al.* 1995). Currently, HD has no known cure and treatments focus on delaying HD-associated symptoms. The causative mutation in HD is expansion of a CAG tract beyond 35 repeats in exon 1 of the *IT15* gene encoding Huntingtin (Htt) (Huntington's Disease Research Collaboration 1993). Similar to other poly(Q)-repeat neurological disorders, abnormal protein conformation(s) secondary to poly(Q) expansion are central to HD pathogenesis (Scherzinger *et al.* 1997; Persichetti *et al.* 1999). The expanded poly(Q) Htt protein can exist in multiple states (Hoffner *et al.* 2005; Nagai *et al.* 2007), including aberrantly folded monomeric forms, oligomeric microaggregates, fibril states, and larger inclusion body aggregates. It is currently unclear which form (s) of mutant Htt are pathogenic and how the abnormally folded protein causes neuronal toxicity.

Poly(Q) expansion leading to aggregation is a common theme in neurodegenerative disorders. Spinocerebellar ataxias (SCA1, SCA2, SCA3/MJD, SCA6, SCA7, and SCA17), spinal bulbar muscular atrophy (SMBA), and dentatorubral pallidoluysian atrophy (DRPLA) all involve poly(Q) expansion, aggregation, and neurodegeneration (Kimura *et al.* 2007). Evidence that aggregates are toxic is mostly correlative for

doi: 10.1534/genetics.111.133710
Manuscript received August 10, 2011; accepted for publication October 27, 2011
Supporting information is available online at http://www.genetics.org/content/suppl/2011/11/17/genetics.111.133710.DC1.
[1]Corresponding author: The Picower Institute for Learning and Memory, 43 Vassar St., 46-3243, Cambridge, MA 02139. E-mail: troy@mit.edu

these diseases, but several studies support the aggregation-toxicity hypothesis. The threshold of poly(Q) repeat number required for the *in vitro* aggregation threshold is similar to that required for disease manifestation (Davies *et al.* 1997; Scherzinger *et al.* 1999). Longer poly(Q) tracts have faster *in vitro* aggregation kinetics and result in earlier disease onset (Scherzinger *et al.* 1999). Similarly, treatments that suppress aggregation, including chaperone overexpression (Carmichael *et al.* 2000) and administration of small molecule aggregation inhibitors (Chopra *et al.* 2007), have been shown to decrease neurodegeneration. Live imaging demonstrates that Htt aggregates can sequester and alter kinetics of trafficked organelles and proteins such as synaptic vesicles (Sinadinos *et al.* 2009) and transcription factors (Chai *et al.* 2002). However, there is also evidence that aggregates may be inert or even neuroprotective. Medium spiny projection neurons of the striatum exhibit fewer Htt aggregates than striatal interneurons, yet are more vulnerable to neurodegeneration in HD (Kuemmerle *et al.* 1999). Additionally, several mouse (Hodgson *et al.* 1999) and *Drosophila* (Romero *et al.* 2008) HD models expressing full-length mutant Htt show selective neurodegeneration and behavioral phenotypes without obvious aggregation. Conversely, the HD mouse model "short-stop" expresses an N-terminal poly(Q)-Htt fragment and displays aggregate formation, but no neuronal dysfunction or degeneration (Slow *et al.* 2005). Indeed, neuronal cell death associated with transient expression of mutant Htt in cultured striatal neurons is inversely proportional to Htt aggregate formation (Arrasate *et al.* 2004), suggesting that inclusion body formation may decrease levels of other toxic forms of Htt and promote neuronal survival. There is also evidence suggesting that oligomers precede aggregate formation and are the toxic species in HD (Lam *et al.* 2008; Lajoie and Snapp 2010). These contradictory results in different cellular contexts and HD models have led to confusion over the toxicity of aggregates and, subsequently, over whether therapeutic approaches in HD should focus on reducing or enhancing aggregate formation.

To further analyze the link between aggregation and toxicity in a model system, we generated transgenic *Drosophila* that express an N-terminal fragment of the human Htt gene with either a pathogenic poly(Q) tract of 138 repeats (HttQ138), corresponding to a juvenile form of HD, or a wild-type nonpathogenic tract of 15 repeats (HttQ15). The Htt transgene used in our analysis is a human Caspase-6 cleavage fragment containing exons 1–12 of the larger Htt locus. Proteolysis of Htt at the Caspase-6 site is an important pathogenic event in HD (Graham *et al.* 2006). Given the uncertainty of cleavage of a larger human Htt transgenic protein in *Drosophila*, the 588-aa fragment represents an attractive biologically relevant cleavage product. The constructs were fused to monomeric red fluorescent protein (mRFP) (Campbell *et al.* 2002) or enhanced green fluorescent protein (eGFP) to allow *in vivo* analysis of aggregate formation and localization. Expression of pathogenic Htt leads to the formation of cytoplasmic aggregates and causes death during the pupal stage. This model provides a tractable system to analyze Htt aggregation kinetics in live animals and to conduct forward genetic screens for modifiers of HD pathology and/or aggregation, allowing us to examine the link between Htt aggregation and neuronal toxicity.

Materials and Methods

Generation of Htt constructs

cDNAs for mRFP-HttQ15, mRFP-HttQ138, eGFP-HttQ15, and eGFP-HttQ138 were subcloned into *Eco*RI (blunt-end ligation) and *Kpn*I sites of the pUAST expression vector. cDNA for eGFP-HttQ138-mRFP was subcloned into the *Xba*I site of the pUAST vector. HttQ15 and HttQ138 cDNAs were kindly provided by Ray Truant (Department of Biochemistry, McMaster University, Hamilton, ON, Canada). cDNA for HttQ96-GFP was kindly provided by David Housman (Center for Cancer Research, Massachusetts Institute of Technology) and subcloned into the *Kpn*I and *Xba*I sites of the pUAST vector. Microinjection of constructs was performed by Genetics Services (Cambridge, MA).

S2 cell transfection and analysis

cDNAs for mRFP-HttQ15 and mRFP-HttQ138 were subcloned into the *Bam*HI and *Eco*RI (blunt-end ligation) sites of the pSR11 S2 transformation vector. To generate constructs expressing mRFP-HttQ15-eGFP and mRFP-HttQ138-eGFP, mRFP-HttQ15 and mRFP-HttQ138 cDNAs were PCR amplified with a forward primer containing an *Eco*RI restriction site and a reverse primer containing a 3′ *Sal*I site and subcloned into the pPL17 vector. Constructs were transfected with 50 μl cytofectene (Bio-Rad, Hercules, CA) into *Drosophila* S2 cells using the Bio-Rad liposome mediated transfection protocol. After 72 hr, 20-μl cell suspensions were fixed with 3.7% formaldehyde in PBT and mounted on slides with 50% glycerol. Images were captured with a Zeiss Pascal laser scanning confocal microscope (Carl Zeiss MicroImaging), using the accompanying Zeiss PASCAL software.

Glue secretion assay

Pupae reared at 25° were isolated shortly after pupariation and placed on slides with the ventral side facing up, using double-sided tape. Visualization was performed on a Pascal confocal microscope (Zeiss).

Drosophila genetics and deficiency screen

Drosophila were maintained on standard medium at 25°. The deficiency collection used in the screen was obtained from the Bloomington Stock Center. Males from deficiency lines on chromosomes II and III were crossed to C155; A37/CyO-GFP or C155; *Df(3)3450/*TM6 virgins, respectively. For the viability screen, F_1 C155/y; Df/Balancer males were mated to homozygous mRFP-HttQ138 high-expression females and the number of F_2 males and females was scored. For the

aggregation screen, F_1 C155/y; Df/Balancer males were mated to homozygous mRFP-HttQ138 low-expression virgins and live wandering third instar larvae expressing mRFP-HttQ138/Df were viewed under a fluorescent stereoscope (Zeiss) to assay changes in aggregation in larval salivary glands. For aggregation formation analysis, the *CCAP*-Gal4 driver was recombined with a *tubulin*-Gal80^{ts} repressor to drive high-expression mRFP-HttQ138 in a temporally restricted manner. mRFP-HttQ138 expression was repressed at 19° until the second instar stage, at which point larvae were moved to 30° to induce expression.

Adult viability analysis

Drosophila viability assays were performed on *white*/C155, HttQ96-GFP/C155, mRFP-HttQ15/C155, mRFP-HttQ138/C155, and mRFP-HttQ138B/C155 flies by daily quantification of lethality for 100 females of each genotype. Flies were aged at 25°, with 20 flies per vial, and transferred every 2–3 days.

Western blot analysis

For HttQ96-GFP Western blots, *Drosophila* were frozen in liquid nitrogen and vortexed. Twenty heads for each indicated genotype were isolated and homogenized in sample buffer, and proteins were separated on 10% SDS–PAGE gels and transferred to nitrocellulose. Blots were incubated with rabbit anti-GFP sc8334 (Santa Cruz Biotechnology) at 1:1000. For eGFP-HttQ138/Q15 and mRFP-HttQ138/Q15, five larvae for each genotype were homogenized in sample buffer and proteins were separated on 10% SDS–PAGE gels. Blots were incubated with mouse anti-Htt MAb2166 (Chemicon) at 1:1000 or anti-Actin (JLA20 antisera; Developmental Studies Hybridoma Bank) at 1:1000. To assay for cleavage of Htt *in vivo*, we crossed UAS-HttQ138-mRFP and UAS-eGFP-HttQ138-mRFP to C155 GAL4 driver strains and prepared head extracts from F_1 progeny expressing Htt. One head extract per lane was loaded and blots were probed with anti-Htt antibodies. Western blots were visualized on a Li-Cor Odyssey infrared imaging system and protein expression was quantified with the accompanying software.

Immunostaining

Wandering third instar larvae reared at 25° were dissected as previously described (Rieckhof *et al.* 2003), except that fixation was limited to 10 min in 4% formaldehyde. Images were captured with a Zeiss Pascal laser scanning confocal microscope (Carl Zeiss MicroImaging), using the accompanying Zeiss PASCAL software.

Quantitative RT-PCR

Quantitative RT-PCR was carried out using an Applied Biosystems (Foster City, CA) 7300 Real-Time PCR system. Total RNA was extracted from 10–15 adult flies per sample, using an RNeasyMini kit (QIAGEN), and treated with DNase I (Ambion) according to the manufacturers' instructions. Single-stranded cDNA was synthesized in a total volume of 20 μl from 1 μg of total RNA, using a High Capacity cDNA reverse transcription kit (Applied Biosystems) according to the manufacturer's protocol. PCR was carried out in triplicate for each of two independent total RNA samples per genotype in optical 96-well plates (Applied Biosystems). The reaction mixtures were as follows: 25 μl of 2× QuantiTect SYBR Green PCR Master Mix (QIAGEN), 300 nM forward primer, 300 nM reverse primer, and 5 μl of single-stranded cDNA (see above) in a total volume of 50 μl. A final dissociation step was carried out to evaluate product integrity, and reaction samples were run on a 1.2% agarose gel and stained with ethidium bromide. The primer sequences were as follows: Act88F (actin) forward 5′-ACTTCT GCTGGAAGGTGGAC-3′ and reverse 5′-ATCCGCAAGGATC TGTATGC-3′.

FRAP and live imaging

Fluorescence Recovery After Photobleaching (FRAP) analysis was carried out using a Zeiss spinning disk confocal microscope with Perkin-Elmer (Norwalk, CT) Velocity 4-D imaging software. Animals were anesthetized with Suprane in a custom chamber that allows imaging through the cuticle of live third instar larvae (Fuger *et al.* 2007) with a 63× oil objective. Camera settings were adjusted so that the aggregate to be bleached was just below saturation. Aggregates were photobleached using 100% laser power at 546 nm for two to five iterations through the entire *z*-plane until they were at 35% of the original fluorescence intensity. *Z*-stack recovery images were recorded at a rate of one per minute for 60 min for FRAP recovery curves at long timescales. An imaging rate of one frame per 10 sec was used for analysis of how individual puncta interact with aggregates and for characterizing aggregate formation events.

Results

A 588-aa N-terminal fragment of pathogenic human Htt reduces Drosophila life span

To explore pathogenic mechanisms in HD, we generated transgenic *Drosophila* that express 588-aa N-terminal fragments of human Htt with either a pathogenic poly(Q) tract of 138 repeats (HttQ138) or a nonpathogenic tract of 15 repeats (HttQ15). While several models of HD have focused on expression of the poly(Q)-containing first exon of Htt alone, the 588-aa fragment is truncated near a number of well-characterized caspase cleavage sites important in the generation of aggregate-forming Htt fragments (Kim *et al.* 2001; Wellington *et al.* 2002; Graham *et al.* 2006). Additionally, many sites of protein interaction that are lost in exon 1 constructs are conserved in the longer 588-aa fragment, including a region of well-conserved HEAT repeats thought to be involved in Htt binding to interaction partners such as HIP1, HAP1, and HIP14 (Harjes and Wanker 2003). Htt was fluorescently tagged with mRFP or eGFP at the N terminus or tagged at both ends with eGFP at the N terminus and mRFP at the C terminus (Figure 1A). For comparison, we generated a transgenic strain expressing exon 1 (81 aa) of

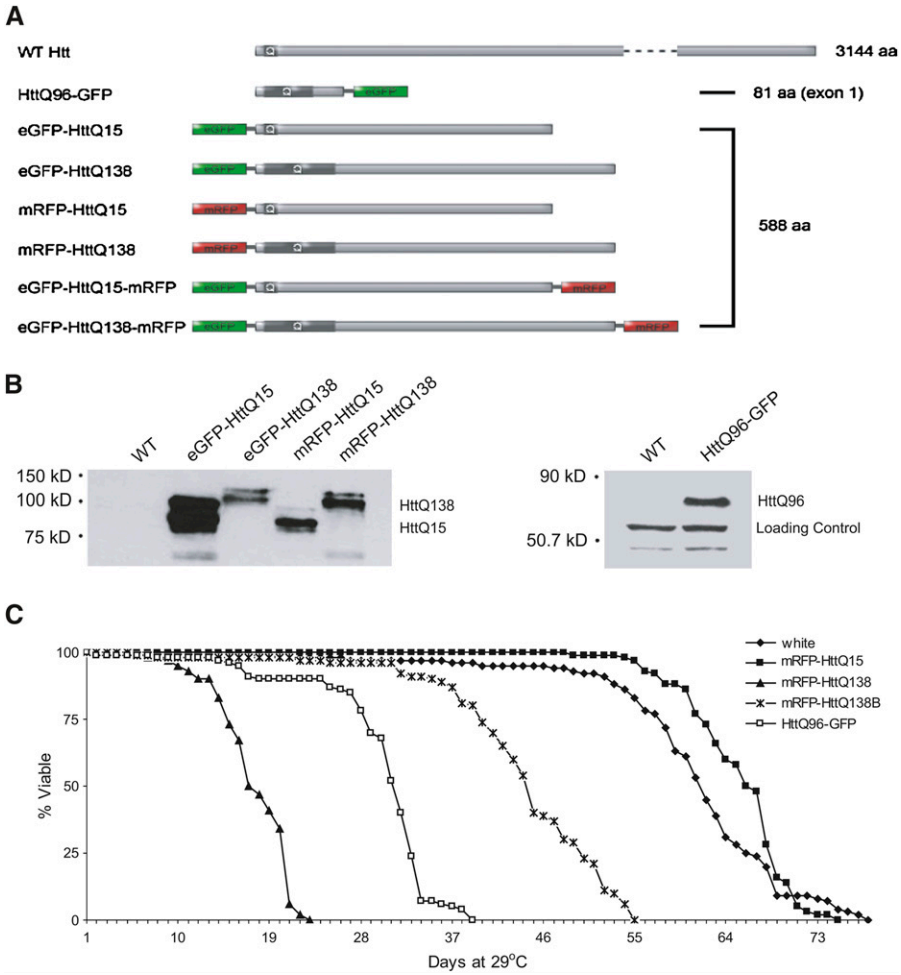

Figure 1 Generation of *Drosophila* transgenic models of HD. (A) The N-terminal fragments of human Htt used for transgenic construction are shown. Poly(Q) tracts and fluorescent tags (mRFP, eGFP) are indicated. The full-sized Htt protein is depicted for comparison. (B) Expression of Htt in control, mRFP-Htt, eGFP-Htt, and HttQ96-GFP strains with transgene expression driven by C155. Western blotting was performed with an antibody to the N terminus of human Htt (mRFP-Htt and eGFP-Htt blot, left) or an antibody to GFP (HttQ96-GFP blot, right). (C) Reduced viability of transgenic strains expressing mutant Htt with a weaker *elav*-GAL4 driver. T_{50} is decreased by >70% in strains expressing mRFP-HttQ138, 30% in strains expressing mRFP-HttQ138B (a lower-expression strain), and 50% in strains expressing HttQ96-GFP, in comparison to control white flies crossed to the same driver.

the human Htt protein with a pathogenic 96Q repeat, fused to GFP at the C terminus (HttQ96-GFP). All constructs were expressed using the UAS-GAL4 system, allowing for temporal and tissue-specific control of transgene expression. To confirm transgene expression, strains were crossed to the neuronal driver *elav*-GAL4 (C155), and Htt expression in offspring was assessed through Western blot analysis with anti-human Htt antibodies (Figure 1B). No Htt expression is detected in control *white* strains crossed to C155, while mRFP-Htt, eGFP-Htt, and HttQ96-GFP lines all demonstrate abundant Htt expression. As expected, the product detected in HttQ15 strains lacking the expanded poly(Q) tract is smaller than that in HttQ138 or HttQ96 strains. These transgenic lines allow imaging of Htt aggregation in live *Drosophila*, providing a resource for following Htt dynamics *in vivo*.

To determine the effects of pathogenic and nonpathogenic Htt expression in *Drosophila*, viability profiles were generated for control and HttQ138-expressing animals. Pan-neuronal expression of mRFP-HttQ138 with C155 causes pharate adult lethality with <1% viable adult escapers. Expression of pathogenic Htt with a weaker *elav*-GAL4 driver results in viable adults that appear behaviorally normal at the time of eclosion. However, several days after eclosion, these adults begin to exhibit motor coordination defects and abnormal grooming behaviors, worsening with age and resulting in premature death. Similar defects occur at a later time in a separate mRFP-HttQ138 insertion line (mRFP-HttQ138B) expressing pathogenic Htt at a lower level, as well as in flies expressing the pathogenic HttQ96-GFP exon 1 protein (Figure 1C). These behaviors are not observed in mRFP-HttQ15–expressing or control *Drosophila*. To quantify the reduction in viability of pathogenic Htt-expressing lines, life span curves were generated for control adults and adults expressing mRFP-HttQ15, mRFP-HttQ138, mRFP-HttQ138B, or HttQ96-GFP (Figure 1C). The T_{50} (age at which 50% of the culture has died) for mRFP-HttQ138 lines is dramatically decreased by >70% in comparison to controls. mRFP-HttQ138B expression results in a 30% decrease in T_{50}, indicating that lethality is correlated with the level of expression of the pathogenic protein. HttQ96-GFP lines also demonstrate a decrease in T_{50} of 50%, suggesting that expression of the expanded poly(Q)-containing first exon of Htt is also toxic. Decreases in T_{50} for all lines expressing fragments of the pathogenic Htt protein, but not the normal protein, indicate that expression of pathogenic Htt results in behavioral dysfunction and reduced life span in *Drosophila*. Although differences in genetic background may contribute to some of the effects on life span,

poly(Q) expansion in Htt consistently reduces life span in our analysis.

Pathogenic Htt forms cytoplasmic aggregates in neuronal and nonneuronal cells in vivo

A hallmark of HD is the formation of intracellular aggregates immunopositive for the pathogenic Htt protein. Aggregates have been found in the nucleus, cell body, and neurites in HD (Difiglia *et al.* 1997). However, it is unknown whether toxic Htt activity occurs in the nucleus, in the cytoplasm, or in both. To determine the intracellular distribution of our pathogenic and nonpathogenic transgenic Htt fragments, *Drosophila* S2 cells were transiently transfected with the mRFP-HttQ15 or mRFP-HttQ138 constructs and fixed cells were imaged by confocal microscopy. While mRFP-HttQ15 demonstrated diffuse cytoplasmic localization, mRFP-HttQ138 formed large, distinct cytoplasmic aggregates (Figure 2A). Neither protein localized to the nucleus.

To assess whether intracellular aggregates are formed *in vivo* by transgenic Htt proteins in *Drosophila*, UAS-mRFP-Htt strains were crossed to lines expressing the *elav*-GAL4 driver. As observed in S2 cells, the nonpathogenic mRFP-HttQ15 remained diffuse throughout the cytoplasm and neurites of neurons in both the CNS (Figure 2B) and the PNS (Figure 2D). In contrast, distinct Htt aggregates were observed throughout the cytoplasm and neurites in lines expressing the pathogenic mRFP-HttQ138 (Figure 2, C and E). To observe subcellular localization in other cell types, mRFP-HttQ15 and mRFP-HttQ138 were driven with a ubiquitous GAL4 driver (*tubulin*-GAL4). In nonneuronal cells, including epidermis (Figure 2F) and salivary glands (Figure 2H), mRFP-HttQ15 localized diffusely in the cytoplasm, while mRFP-HttQ138 formed cytoplasmic aggregates (Figure 2, G and I). Nuclear aggregates were not observed in any cell type. These results suggest that Htt fragments induce pathology primarily through a cytoplasmic localization in this *Drosophila* model.

Mutant Htt causes defects in salivary gland glue secretion in Drosophila

To determine whether HttQ138 expression might cause defects in nonneuronal tissues, we tested whether Htt expression in larval salivary glands causes cellular dysfunction. We analyzed secretion of the GFP-tagged salivary gland glue protein Sgs3 (Biyasheva *et al.* 2001) in controls and animals expressing mRFP-HttQ15 or mRFP-HttQ138 (Figure 3). During normal puparation, *Drosophila* secretes ecdysteriod-induced glue granules that mediate attachment of the developing pupal case to surfaces. While glue secretion is evident in both control and mRFP-HttQ15–expressing pupae (Figure 3, A and B), secretion is decreased in pupae expressing mRFP-HttQ138 (Figure 3C). Normal third instar larval salivary gland cells are filled with glue proteins (Figure 3D) that are depleted during pupariation (Figure 3E). In contrast, the pupal salivary glands of mRFP-HttQ138–expressing larvae retain glue (Figure 3F), suggesting salivary gland dysfunction mediated by the cytoplasmic accumulation of mutant Htt.

The 588-aa fragment of pathogenic human Htt does not produce nuclear cleavage products in Drosophila

Mutant forms of Htt have been reported to undergo cleavage by caspases and calpains to generate smaller N-terminal fragments that can be observed in the nucleus and cytoplasm (Kim *et al.* 2001; Lunkes *et al.* 2002; Wellington *et al.* 2002; Gafni *et al.* 2004). To determine whether cleavage of the N-terminal 588 aa of Htt occurs in our *Drosophila* model to generate smaller fragments that might localize to the nucleus, S2 cells were transiently transfected with 588-aa Htt constructs labeled with eGFP at the N terminus and mRFP at the C terminus. Complete colocalization of the eGFP and mRFP signals was observed for both the normal eGFP-HttQ15-mRFP fragment (Figure 4A) and the pathogenic eGFP-HttQ138-mRFP fragment (Figure 4B). These results suggest that cleavage of Htt does not occur in the context of *Drosophila* S2 cells or, alternatively, that any cleaved N- and C-terminal fragments of Htt remain colocalized in the cytoplasm.

To assess whether cleavage and separation of N- and C-terminal fragments of Htt occur *in vivo*, we generated transgenic strains expressing the double-labeled pathogenic Htt fragment eGFP-HttQ138-mRFP. As observed in the S2 cell model, eGFP and mRFP signals colocalized in all tissues studied, including CNS neurons (Figure 4C), salivary gland cells (Figure 4D), and epidermal cells (Figure 4E), suggesting that pathogenic Htt is unlikely to be cleaved *in vivo* in *Drosophila*. Neither N- nor C-terminal fragments of Htt are observed in the nucleus. To further test whether cleavage occurs *in vivo*, we performed Western analysis with anti-Htt antibodies to probe for breakdown products that would result from cleavage of the protein. As shown in Figure 4F, no differential cleavage products were observed by Western analysis in head extracts prepared from animals expressing HttQ138-mRFP *vs.* those from animals expressing eGFP-HttQ138-mRFP. Thus, the pathogenic Htt-mediated toxicity seen in our *Drosophila* HD model does not appear to require Htt cleavage or nuclear entry and reflects an effect of the 588-aa fragment in the cytoplasm.

Exon 1 of pathogenic Htt forms cytoplasmic and neuritic aggregates

Many classic HD models express exon 1 of the mutant protein (Davies *et al.* 1997; Jackson *et al.* 1998; Krobitsch and Lindquist 2000; Tagawa *et al.* 2004), which is capable of forming inclusions postulated to play a role in HD pathology (Davies *et al.* 1997; Becher *et al.* 1998). To determine whether the *in vivo* subcellular localization of the 81-aa exon 1 fragment of pathogenic human Htt (HttQ96-GFP) differs from that of the 588-aa pathogenic Htt fragment in our *Drosophila* model, HttQ96-GFP–expressing third instar larvae were imaged using confocal microscopy. In both neuronal and nonneuronal cell types, HttQ96-GFP formed

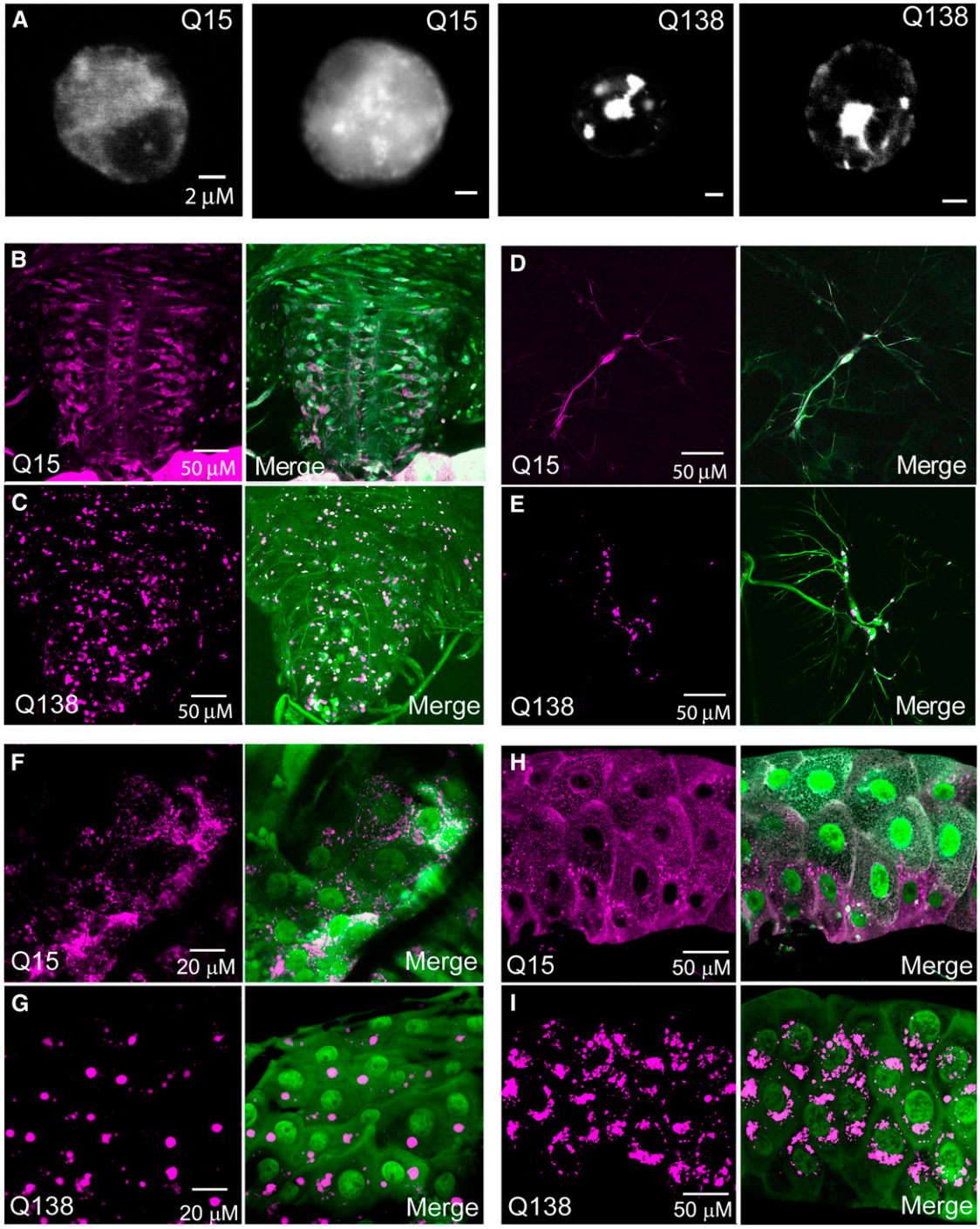

Figure 2 Cytoplasmic aggregation of mRFP-HttQ138 in neuronal and nonneuronal tissues. (A) Htt localization in *Drosophila* S2 cells transiently transfected with mRFP-HttQ15 or mRFP-HttQ138. mRFP-HttQ15 is found diffusely throughout the cytoplasm, while mRFP-HttQ138 forms cytoplasmic aggregates. Bar, 2 μm for each panel. (B) Visualization of mRFP-HttQ15 (magenta) and GFP with a nuclear localization signal (nls) (green) in third instar larvae with transgene expression driven by C155. mRFP-HttQ15 is diffusely localized in the cytoplasm of CNS neurons in the ventral nerve cord. (C) Visualization of mRFP-HttQ138 (magenta) and GFP-nls (green) in CNS neurons of third instar larvae with transgene expression driven by C155. Unlike mRFP-HttQ15, mRFP-HttQ138 forms cytoplasmic aggregates throughout the cell bodies of ventral nerve cord neurons. (D and E) Visualization of mRFP-Htt in peripheral multidendritic neurons. While mRFP-HttQ15 exhibits diffuse cytoplasmic localization, mRFP-HttQ138 is found in cytoplasmic aggregates throughout the cell body and neurites. (F–I) Expression of mRFP-Htt (magenta) and GFP-nls (green) driven by the *tubP*-GAL4 driver in the epidermis (F and G) and salivary gland (H and I). In all cases, mRFP-HttQ15 is diffuse throughout the cytoplasm, while mRFP-HttQ138 forms cytoplasmic aggregates.

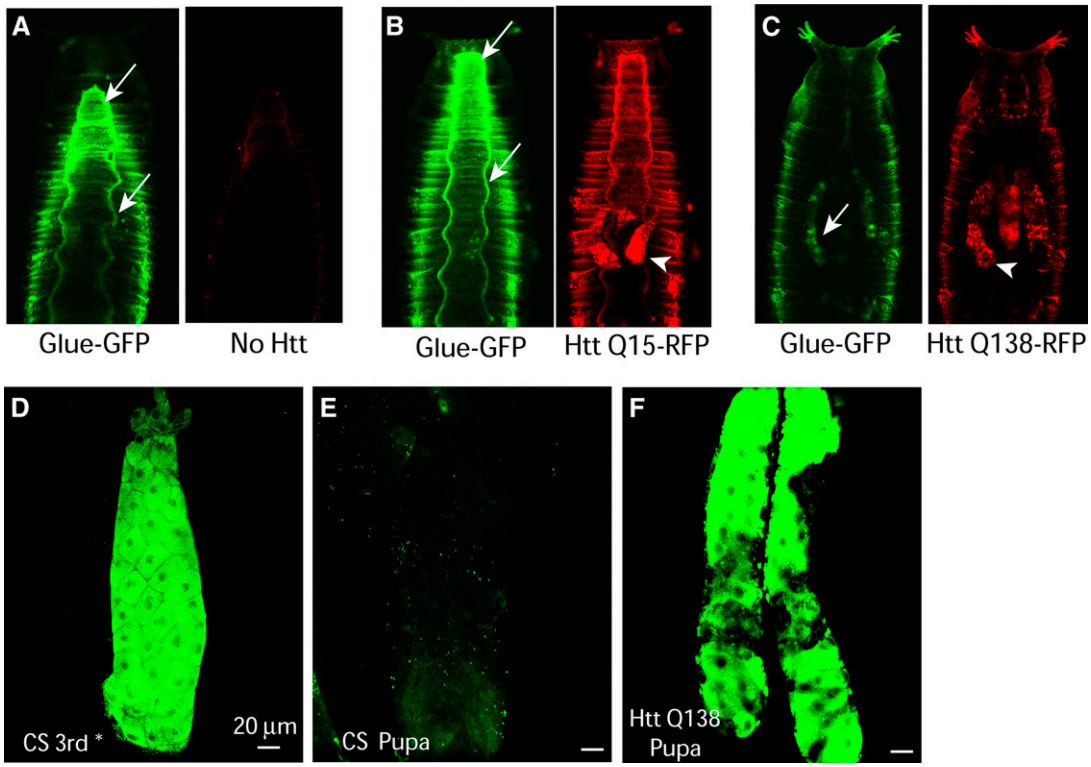

Figure 3 Salivary gland glue secretion is defective in *Drosophila* expressing mRFP-HttQ138. (A) Pupae were removed from vials of CS (A), Htt-Q15 (B), or HttQ138 (C) animals expressing the Sgs3 GFP-tagged glue protein. Confocal images of Sgs3-GFP fluorescence are shown in the left panels and mRFP-Htt fluorescence in the right panels. (A) The Sgs3-GFP glue protein can be readily seen in the left panel lining the exterior surface of the pupal case (arrows) following secretion from salivary glands. CS animals do not express Htt-mRFP, with only minor autofluorescence visible in the red channel (right panel). (B) Glue secretion (arrows) is not disrupted in pupae that express mRFP-HttQ15, which localizes diffusely in the salivary gland (arrowhead). (C) Glue secretion is decreased in pupae expressing mRFP-HttQ138, with the Sgs3-GFP protein largely retained in salivary glands (arrows). Aggregation of mRFP-HttQ138 in the pupal salivary glands is noted by the arrowhead in the right panel. (D and E) Sgs3-GFP is abundant in CS third instar larval salivary glands before pupation (D) and depleted from salivary glands following secretion during pupation (E). (F) Sgs3-GFP is retained in pupal salivary glands of mRFP-HttQ138–expressing animals. Bars, 20 μm.

distinct cytoplasmic aggregates similar in appearance and localization to those formed by the 588-aa mRFP-HttQ138 protein. GFP-labeled aggregates are found in the cytoplasm of salivary gland cells (Figure 5B) and CNS (Figure 5D) and PNS (Figure 5G) neurons, while no aggregates are observed with expression of a UAS-GFP construct alone (Figure 5, A, C, and F). As observed with the 588-aa fragment, the exon 1 fragment also forms aggregates in axons (Figure 5E) and localizes at nerve terminals. The localization of both 588-aa and 81-aa pathogenic Htt fragments indicates that the neurodegenerative effects induced by these toxic Htt forms are independent of Htt nuclear accumulation in *Drosophila*. In addition, targeting sequences in exon 1 of Htt are sufficient to localize the protein to neurites in our model.

Kinetics of HttQ138 aggregate formation

To examine how Htt aggregates form, we visualized mRFP-HttQ138 dynamics in live larvae. We expressed mRFP-HttQ138 using *CCAP*-GAL4 that expresses in a single neuron per hemisegment (Park *et al.* 2003; Vomel and Wegener 2007). This driver allows single-cell resolution for assaying how soluble HttQ138 interacts with larger aggregates. Time-lapse confocal imaging in third instar larval motor neurons expressing mRFP-HttQ138 demonstrates that large aggregates are immobile over a 2-h imaging session. FRAP analysis reveals that HttQ138-positive photobleached aggregates continually add new HttQ138 particles, with a 40% recovery of original fluorescence within 50 min (Figure 6, A–C, Supporting Information, File S1). Two general types of recovery were observed. Larger HttQ138 aggregates tend to recover more quickly by trapping Htt particles (rightmost aggregate in File S1). A second class of aggregates recovers more slowly and displays a gradual and uniform increase in brightness (left three aggregates in File S1). To determine whether the rapid FRAP in axons was due to increased flux of HttQ138 mediated by delivery of new particles by fast axonal transport (FAT), we compared FRAP rates of aggregates in axons to those in neuronal cell bodies aggregates where HttQ138 movement is dictated largely by diffusion. We did not observe a significant difference in aggregation kinetics in these two compartments, indicating that axonal aggregation kinetics are not strictly dependent on FAT (Figure 6B).

We next examined the kinetics of *de novo* HttQ138 aggregate formation in our model *in vivo*. During our time-lapse

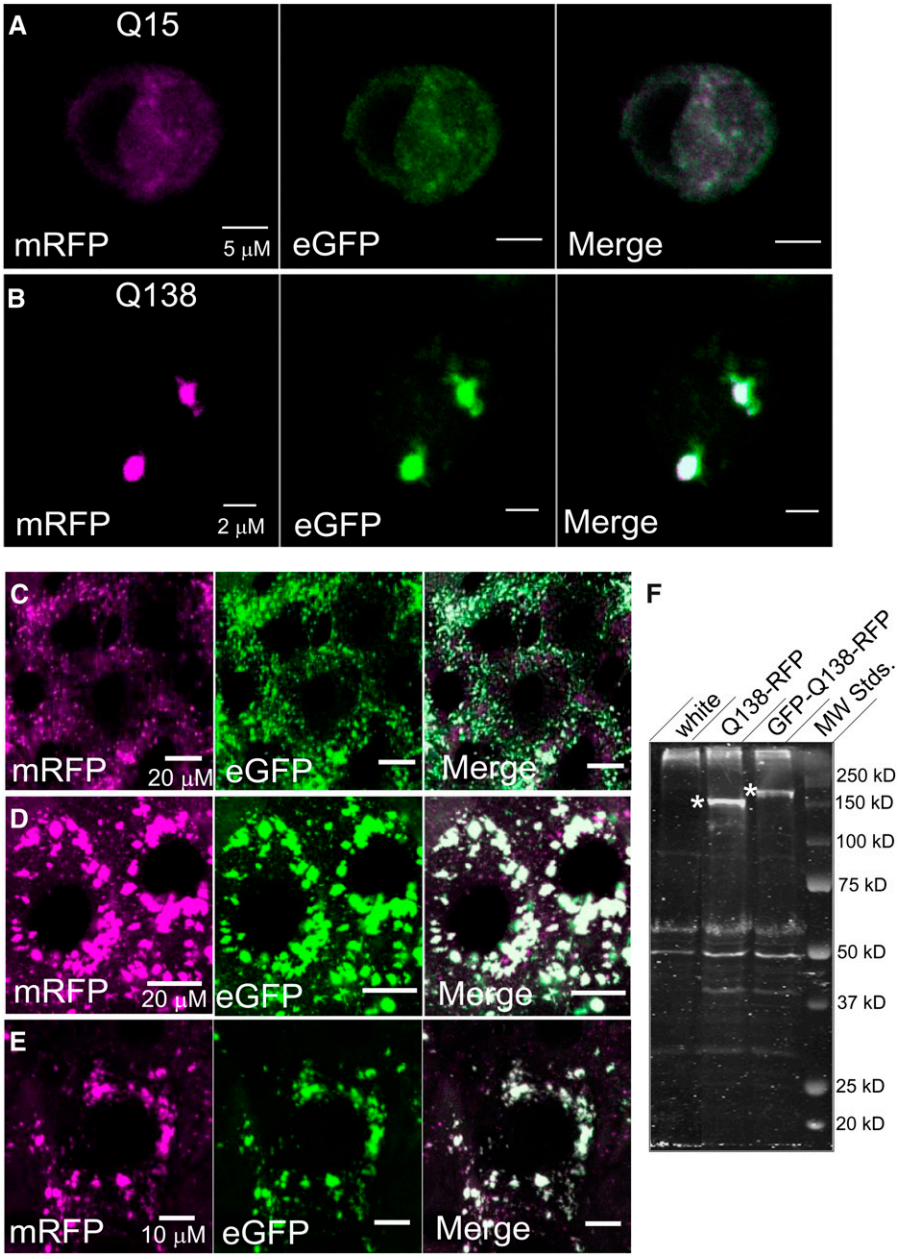

Figure 4 The 588-aa fragment of mutant human Htt does not undergo cleavage in *Drosophila*. (A and B) Transient transfection of *Drosophila* S2 cells with eGFP-HttQ15-mRFP (A) or eGFP-HttQ138-mRFP (B) demonstrates no separation of eGFP (green) and mRFP (magenta) signals, suggesting that the mutant Htt protein does not undergo cleavage in S2 cells. (C–E) Visualization of signal localization in third instar larvae with expression of eGFP-HttQ138-mRFP driven by C155 shows no separation of eGFP (green) and mRFP (magenta) signals in CNS neurons (C), salivary gland cells (D), or epidermal cells (E). (F) Western analysis of brain extracts from control *white* animals and animals expressing Q138-mRFP or eGFP-Q138-mRFP, showing expression of the Htt protein (asterisks). Immunoblotting with anti-Htt antibodies reveals no differential breakdown product in the double-labeled strain compared to single-labeled lines or control animals that do not express Htt.

imaging sessions in third instar larvae, we did not observe new aggregates forming. We attempted to visualize aggregate formation in younger animals, but numerous aggregates were already present at the first instar larval stage. It appeared that aggregates that formed early in development grew, but that new aggregates rarely formed in the presence of preexisting ones. To bypass this problem, we used the temperature-sensitive GAL80 repressor to restrict expression of mRFP-HttQ138 through the second instar stage. Expression of mRFP-HttQ138 with the *CCAP*-GAL4 driver was repressed by $GAL80^{ts}$ at 18° until the larvae reached third instar. We then turned on HttQ138 expression by shifting animals to the $GAL80^{ts}$ restrictive temperate of 30°. Two hours after induction of expression, a low level of diffuse mRFP-HttQ138 was observed in the salivary gland. By 4 hr, small Htt aggregates were observed forming in the salivary gland (Figure 7). After 8 hr of expression, diffuse mRFP-HttQ138 was seen in neuronal cell bodies in the ventral nerve cord, as well as in the proximal regions of axons. By 12 hr, aggregates were seen forming in axons and cell bodies, while salivary gland aggregates increased in size. During the window from 12 to 24 hr after induction, aggregates became larger and more numerous (Figure 7). Beyond 12 hr postinduction, HttQ138 aggregates began growing in size rather than number. The increase in aggregated mRFP-HttQ138 was accompanied by a decrease in the soluble fraction of the protein. We also examined the effectiveness of reducing aggregation by turning off expression of the mRFP-HttQ138 transgene after aggregates had formed, assaying whether cells had the ability to remove aggregates without new HttQ138 expression. After a 24-hr

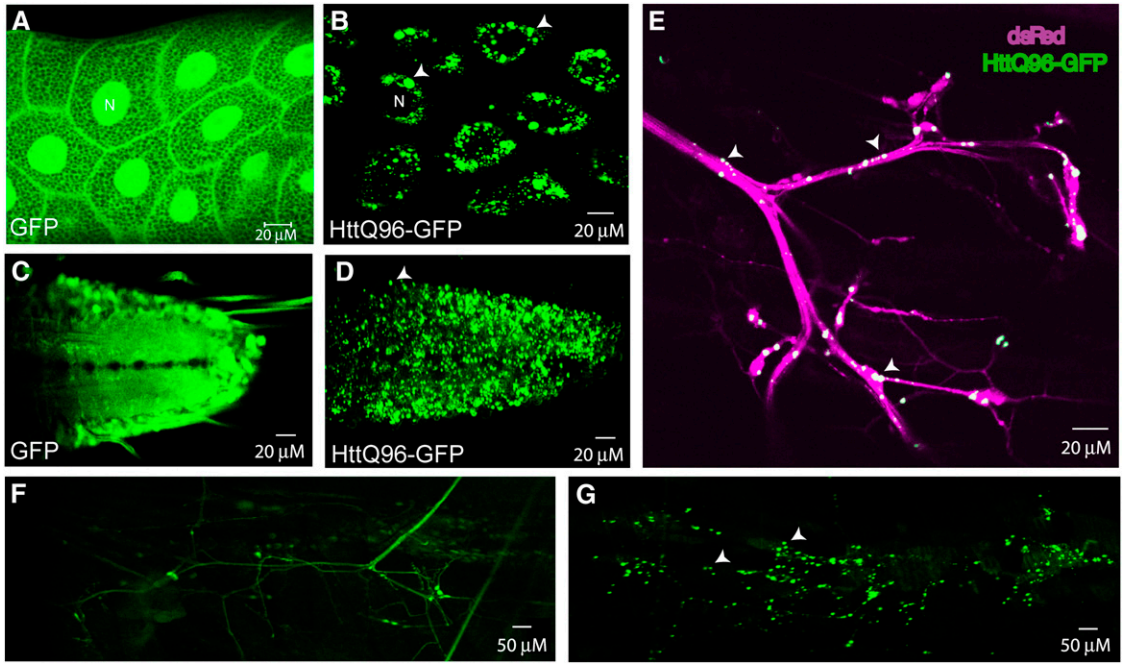

Figure 5 Cytoplasmic aggregation of HttQ96-GFP in neuronal and nonneuronal tissues. (A) Visualization of UAS-GFP (green) expression alone in the salivary gland shows localization to the cytoplasm and nucleus (indicated by N). (B) Visualization of HttQ96-GFP (green) in the salivary gland. Unlike GFP, HttQ96-GFP forms cytoplasmic aggregates in the salivary gland. The nucleus is indicated by N, with aggregates indicated by arrowheads. (C and D) Visualization of GFP alone or HttQ96-GFP in CNS neurons of the ventral nerve cord. GFP is diffusely localized in CNS neurons, while HttQ96-GFP forms aggregates. Several Htt aggregates are denoted by arrowheads. (E) HttQ96-GFP aggregates (green, indicated by arrowheads) are found in axons labeled as expressing dsRed (magenta) in C155, UAS-dsRed, UAS-HttQ96-GFP larvae. (F) In peripheral axons and synapses of C155, UAS-GFP larvae, GFP (green) is diffuse in the cytoplasm. (G) In contrast, HttQ96-GFP (green) is found in cytoplasmic aggregates (indicated by arrows) in peripheral axons and synapses in C155, UAS-HttQ96-GFP larvae.

pulse of mRFP-HttQ138 expression followed by 72 hr of recovery, we observed a reduction in the size and number of aggregates present (Figure 7). We conclude that new aggregates can form in neurons within 12 hr, while preexisting aggregates rapidly accumulate new HttQ138 protein within minutes. In addition, in the absence of new Htt protein synthesis, neurons are capable of reducing preexisting Htt aggregate size over time.

mRFP-HttQ138–induced lethality can be rescued by heterozygous disruption of single loci

To further define the role of aggregation in HD pathology, we performed forward genetic screens for suppressors of HttQ138-induced lethality or suppressors of HttQ138 aggregation. For the first screen to identify lethality suppressors, we employed a dominant suppressor strategy with the *Drosophila* autosomal deficiency (Df) set to identify chromosomal regions containing loci that could dominantly rescue mRFP-HttQ138–induced lethality. We reasoned that loci identified in a haplo-insufficiency screen might represent attractive targets for ameliorating HD pathology, as a 50% decrease in protein activity might require only partial reduction of the protein's function through pharmacological approaches. We obtained the Df kit for chromosomes II and III from the Bloomington Stock Center, which contains 160 Df lines that cover ~80% of the *Drosophila* genome. We crossed Df/Balancer males to females carrying the *elav*-GAL4 driver homozygous on the X chromosome (C155) and a marked Balancer, with *CyO* for the second chromosome and *Sb* or *Hu* for the third chromosome. F_1 C155/y; Df/Bal offspring were then mated to homozygous mRFP-HttQ138 high-expression females. Under normal conditions, expression of mRFP-HttQ138 driven by C155 caused pharate adult lethality. We screened for Dfs that rescued this lethality, comparing the number of adult females expressing mRFP-HttQ138 to that of males not expressing the HttQ138 transgene. Deficiencies that dominantly increased the ratio of mRFP-HttQ138–expressing females by 10-fold (female/male ratio = 0.1) were identified as hits. We identified 11 large Dfs, each removing ~100 genes, that suppressed HttQ138-induced lethality, indicating the presence of multiple potential targets that can modify HttQ138 toxicity in a dominant manner (Figure 8A, Table S1). Ten of 11 deletions gave a partial rescue of viability, increasing the number of escapers to ~20–30% of that expected for a full rescue. The viable animals displayed motor defects, as they were unable to climb the walls of the vials or mate, and most died within several days of eclosion, indicating partial rescue. One of the 11 large deletions, *Df(3L)vin7* showed a near complete rescue of viability at eclosion. C155; *Df(3L)vin7*/mRFP-HttQ138 animals showed less severe motor defects

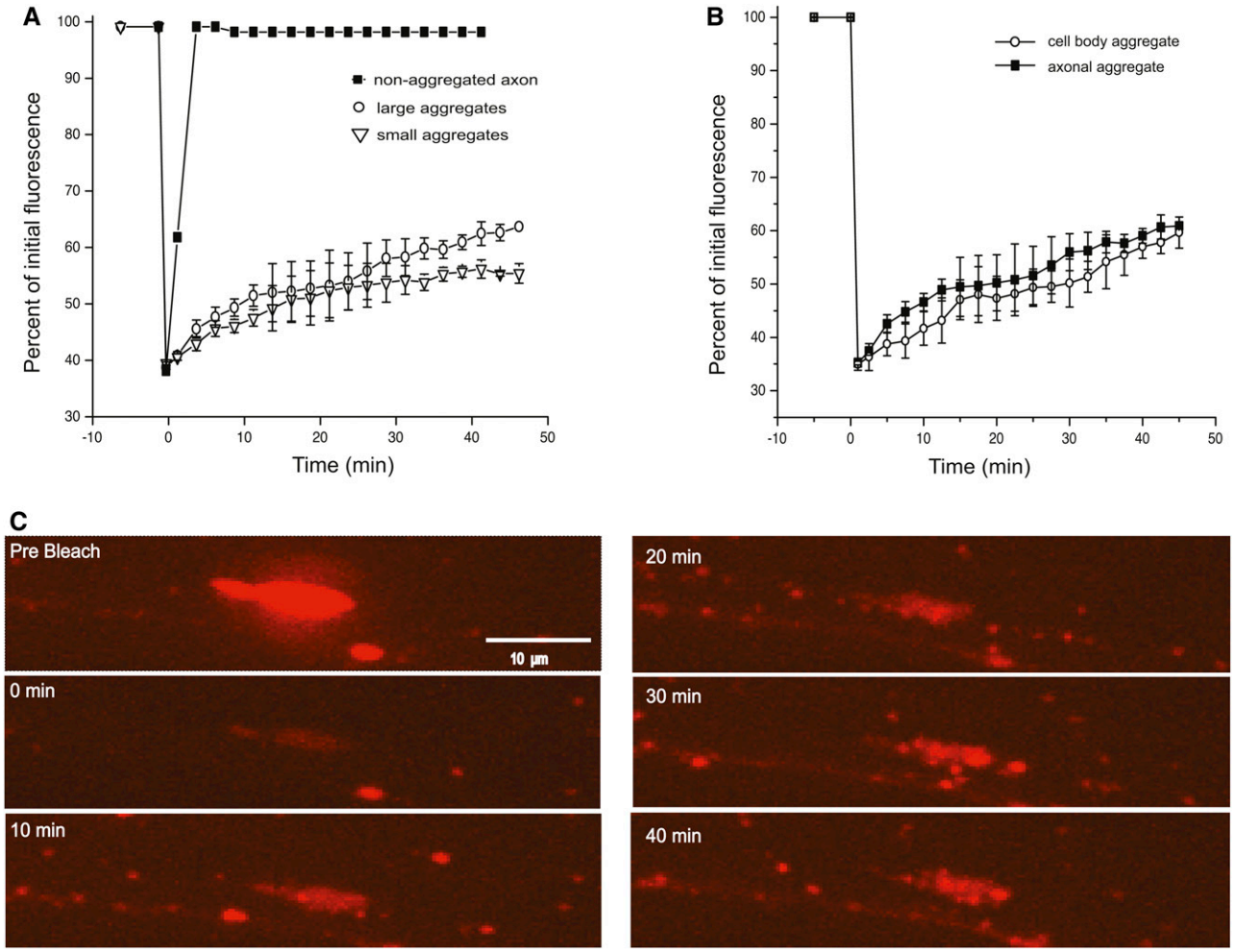

Figure 6 FRAP microscopy shows that mRFP-HttQ138 aggregates continue to accumulate HttQ138 in live anesthetized third instar larval axons. (A) Averaged traces comparing FRAP rates of regions of axons with no aggregates, large aggregates that equal or exceed the diameter of the axon, and smaller aggregates less than the diameter of the axon. While regions without aggregates recover quickly due to fast axonal transport, large and small HttQ138 aggregates recover at a slower rate, but to a greater level. The graph shows percentage of initial fluorescence, not total fluorescence. Larger aggregates recover at a greater rate than smaller ones. (B) HttQ138 aggregation kinetics demonstrated by FRAP in different regions of the motor neuron. (C) Time-lapse images of a FRAP experiment showing recovery of an aggregate over 40 min in a live anesthetized third instar larval motor neuron axon.

than other rescuing Dfs, but were unable to climb the vial walls and lived ~10 days posteclosion.

Reduction of HttQ138 expression and aggregation increases viability in mRFP-HttQ138–expressing Drosophila

In addition to the viability screen, we conducted a screen for suppressors of aggregation. The same mating scheme was used in both screens. However, the aggregation screen used the lower-expression adult-viable mRFP-HttQ138B insert, instead of the pharate lethal high-expression mRFP-HttQ138 line. We reasoned the lower-expression line would represent a more sensitized system to identify potentially weak aggregation suppressors that might not be found in strong expression strains. Live wandering third instar larvae expressing mRFP-HttQ138 and hetererozygous for each Df were screened under a fluorescent microscope for changes in aggregation. We focused on Htt aggregation within the salivary gland, as these large cells were easily visualized in live animals. We screened for changes in size, density, or brightness of perinuclear mRFP-Htt salivary gland aggregates. Four large deletions, (*Df(2R)59AD*, *Df(2R)AA21*, *Df(2R)cn9*, and *Df(3L)vin7*) caused a reduction in aggregate density in the salivary gland (Figure 8, B–F). Interestingly, each of these aggregation suppressors was independently identified in the viability screen. Thus, reducing aggregation in our screen was always associated with increased viability. We did not identify any hits that reduced aggregation without increasing viability, suggesting that aggregates may represent a toxic species in this model. While *Df(2R)59AD* reduced the density and size of salivary gland aggregates, *Df(2R)cn9*, *Df(3L)vin7*, and *Df(2R)AA21* were most effective in reducing aggregation, with the mRFP-Htt Q138 pattern appearing as diffuse as the nonpathogenic mRFP-HttQ15.

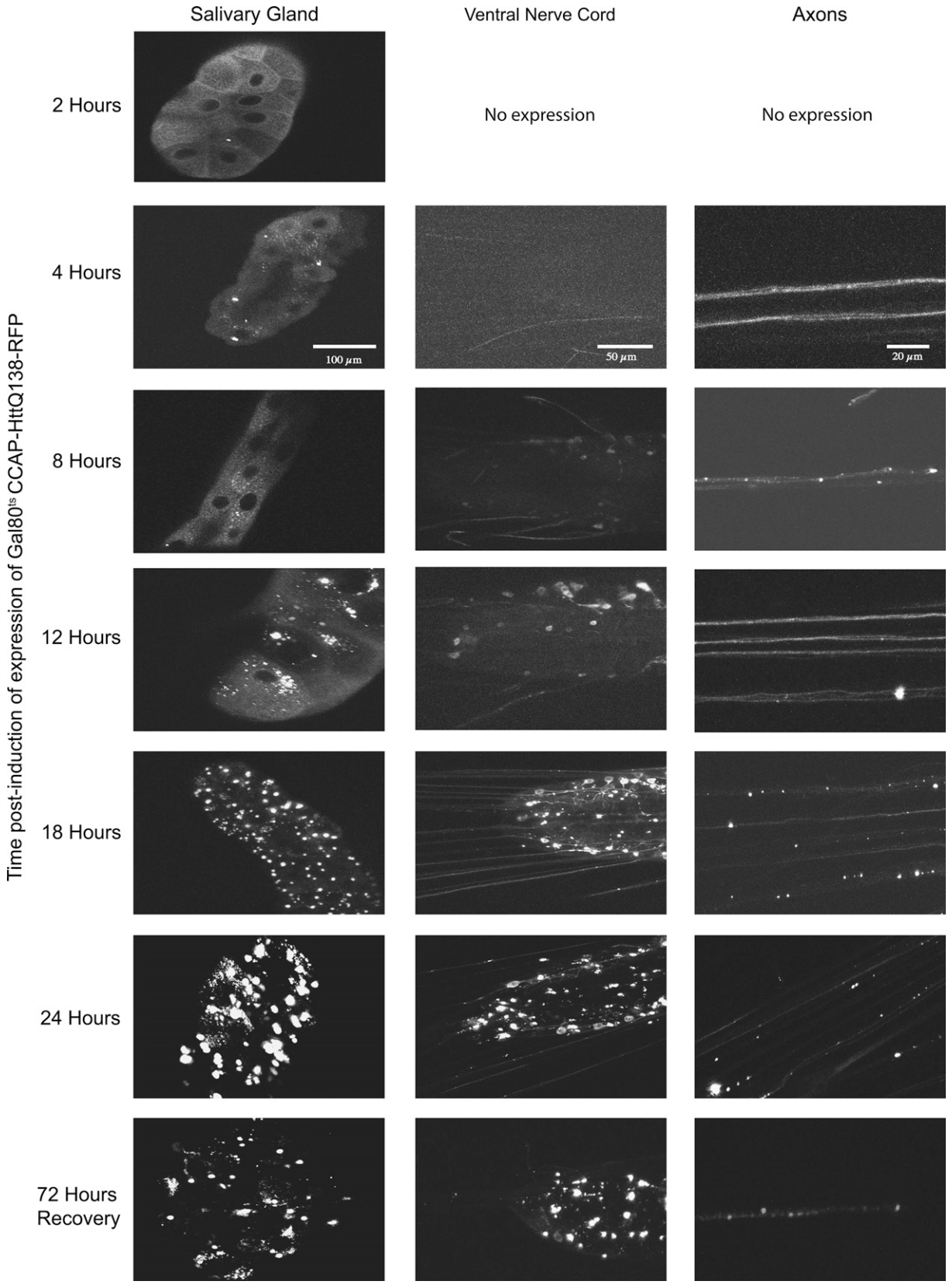

Figure 7 Acute induction of mRFP-HttQ138 expression by *CCAP*-GAL4 shows the pattern of aggregate formation in salivary glands, ventral nerve cord, and axons over 24 hr. Expression of UAS-HttQ138 was repressed using *tubulin*-Gal80^{ts} at 19° during early development. Animals were moved to 30° for the designated time, dissected, and imaged immediately to avoid fixation artifacts.

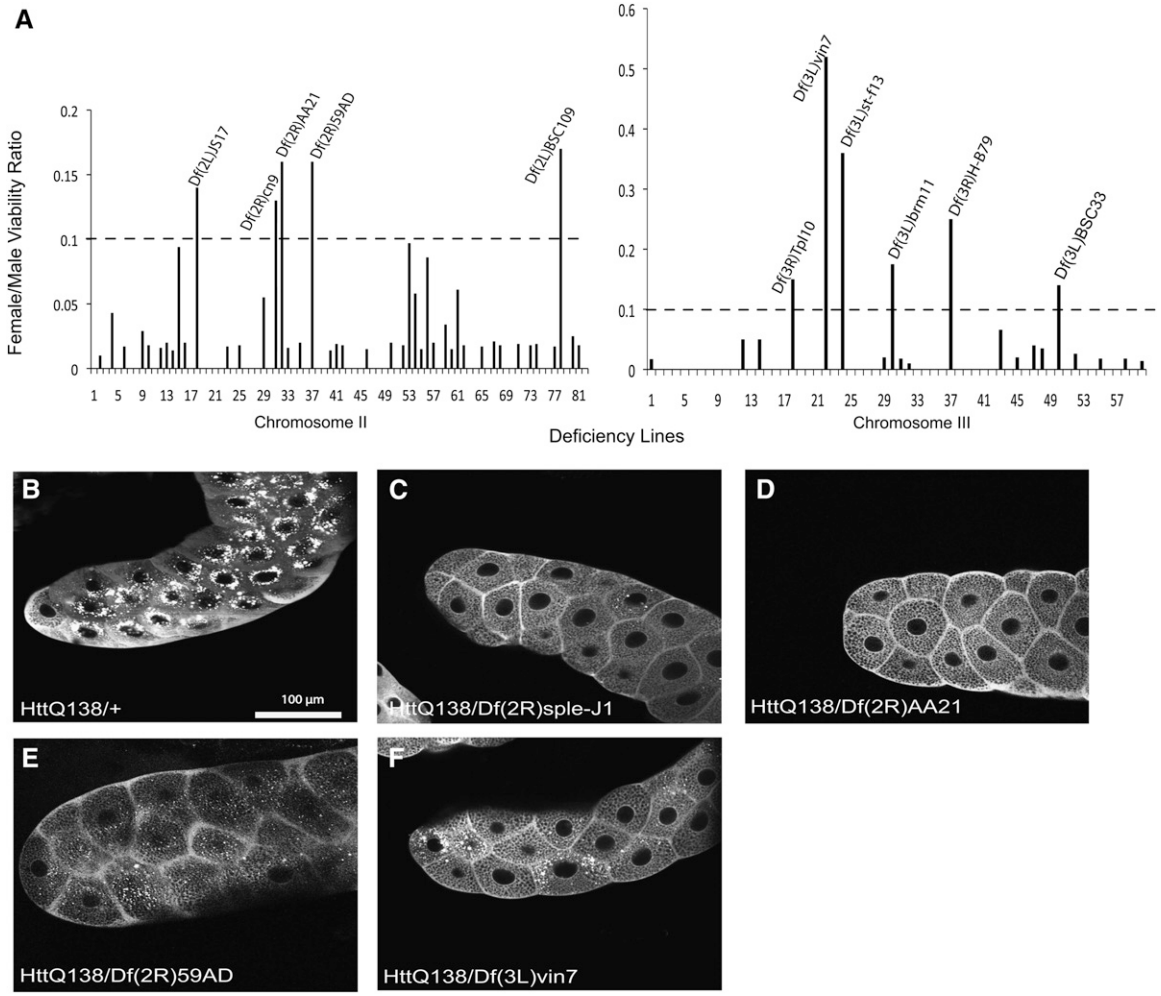

Figure 8 Suppression of lethality with a Df haploinsufficiency screen. (A) Male/female viability ratio of mRFP-HttQ138–expressing Df lines. Homozygous mRFP-HttQ138 females were crossed to C155/y; Df/Bal males for 81 Df lines on chromosome II and 60 Df lines on chromosome III. Few female escapers expressing mRFP-HttQ138 are ever seen in control crosses (male/female ratio = 0.01). All Dfs with a viability ratio >0.1 were identified as hits. (B–F) Confocal images of mRFP-HttQ138 aggregates in the salivary glands of third instar larvae from controls (B) and animals heterozygous for *Df(3L)vin7* (C), *Df(2R)sple-J1* (D), *Df(2R)AA21* (E), and *Df(2R)59AB* (F). Bars, 100 μm.

We attempted finer mapping for each larger Df to define the smallest relevant genetic interval. We were able to map the *Df(2R)59AD* interval to a region uncovered by *Df(2R)59AB*, which deletes ~20 genes. The larger *Df(2R)cn9* was subdivided to a critical region uncovered by *Df(2R)sple-J1*, which removes ~39 genes.

To determine whether suppression of aggregation was associated with a change in mRFP-HttQ138 expression, we quantified Western blots of flies expressing mRFP-HttQ138 with C155 in the Df background (Figure 9, A and B). As a control for UAS-GAL4 transgene regulation, we also quantified expression of UAS-CD8-GFP in the Df backgrounds (Figure 9C). All four deletions that reduced aggregation resulted in reduced mRFP-HttQ138 and CD8-GFP protein expression. However, two single gene suppressors (*lab*[14], PBc02324; see below) had no effect on salivary gland aggregation or transgenic protein expression by Western analysis. To further characterize the suppressors, we measured HttQ138 mRNA levels using semiquantitative RT-PCR. Despite showing distinct effects on protein level, all Dfs decreased HttQ138 mRNA levels. These results are consistent with the observation that Htt aggregation is strongly influenced by expression levels of the protein and that toxicity in our model correlates with HttQ138 expression level (Figure 1C).

We next determined whether the reduction in salivary gland HttQ138 aggregates and suppression of lethality by these Dfs resulted in alteration in the subcellular distribution or density of Htt aggregates in peripheral nerves. Htt aggregates in axons have been suggested to cause axonal transport defects and contribute to HD pathogenesis (Li *et al.* 1999, 2001; Gunawardena *et al.* 2003; Lee *et al.* 2004). We found a significant ($P < 0.05$) decrease in the number of mRFP-HttQ138 aggregates >1 μm diameter in axons in the *Df(3L)vin7* background, but no change in the other Dfs (Figure 10). Interestingly, *Df(3L)vin7* had the strongest effect on suppressing lethality (Figure S1) and

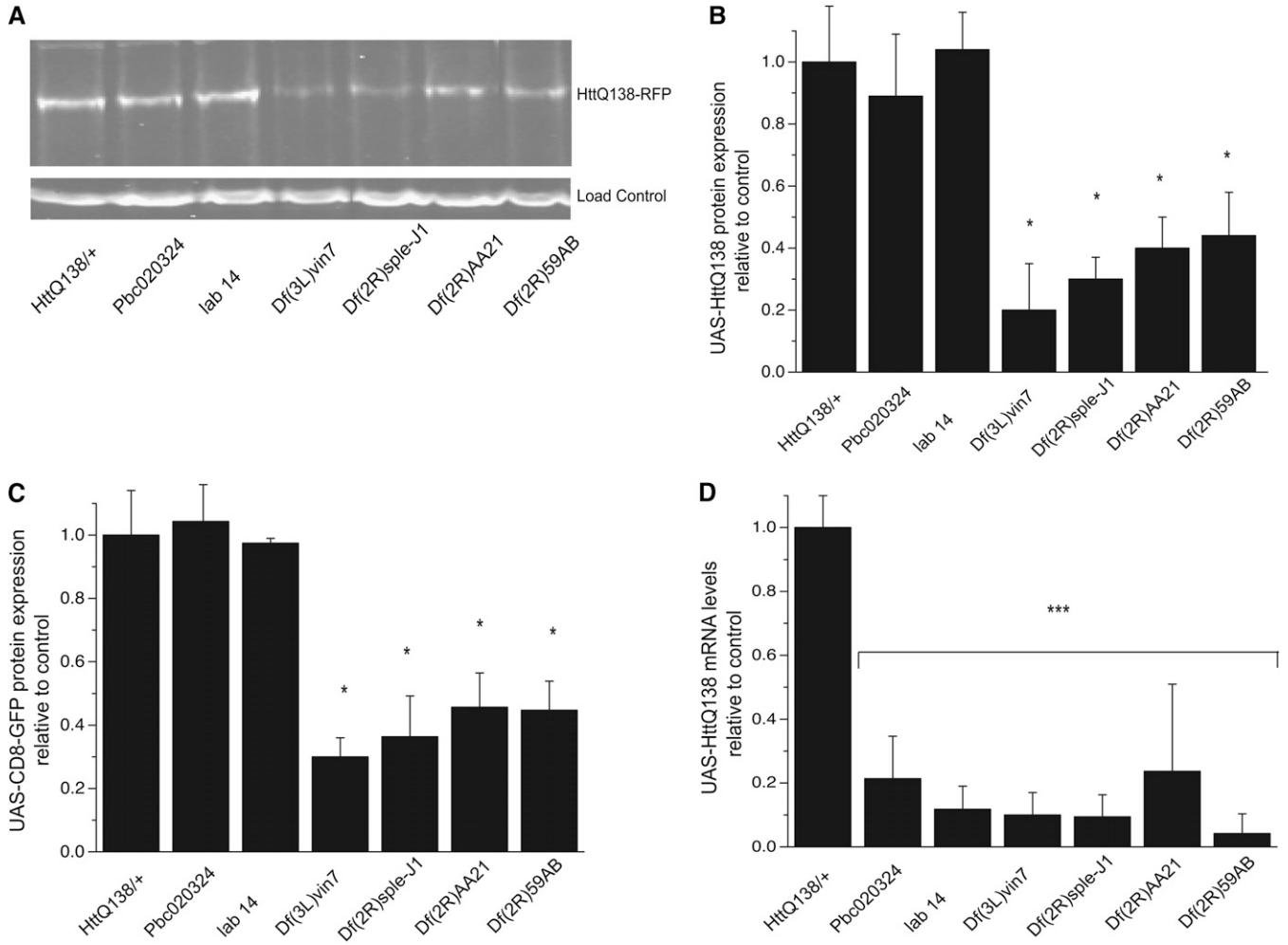

Figure 9 Quantification of transgenic Htt expression. (A) Western blot with C155-driven HttQ138 expression in control (*white*) and the indicated genotypes from pupal head extracts probed with anti-Htt antibodies and control anti-actin antibodies. (B) Quantification of C155-driven HttQ138 protein expression in control (*white*) and the indicated genotypes from pupal head extracts. The control containing C155; UAS-mRFP-HttQ138 was normalized to one for the genotypic comparisons. (C) Quantification of C155-driven GFP-CD8 expression in control (*white*) and the indicated genotypes from adult head extracts by Western blot analysis with anti-GFP antibodies. (D) HttQ138 mRNA levels were measured in pupal head extracts by quantitative RT-PCR and normalized to control (*white*) expression. Error bars indicate SEM. $*P < 0.05$ by Student's *t*-test.

improving motor performance in HttQ138-expressing animals. We also analyzed Syt 1 distribution along axons, which we have previously observed to coaggregate with Htt in axonal aggregations (Lee *et al.* 2004), while remaining diffuse in axons from controls or HttQ15-expressing animals. Abnormal aggregation of Syt 1 was still observed in the rescued animals (Figure 10, A–G), indicating that although the Dfs reduced aggregation in salivary glands and suppressed lethality, they did not prevent axonal aggregation of HttQ138. The identification of dosage-sensitive suppressors of mutant Htt toxicity that reduce lethality without disrupting aggregation suggests that pathways downstream of aggregate formation can be targeted for neuroprotection in HD. The differences in HttQ138 mRNA levels *vs.* HttQ138 aggregates also suggest that subtle changes in transcript level can have a dramatic effect on the concentration reached within a cell that is required to trigger aggregation.

Mapping of suppressors of HttQ138-induced lethality

To begin identifying loci that underlie suppression of HttQ138-induced phenotypes, we attempted finer mapping of hits from the viability and aggregation screen by testing smaller and overlapping Dfs within these regions using stocks available from the Bloomington Stock Center (Table S2). In many cases, coverage across the original Df region was not sufficient to map suppression to individual loci. It is also possible that the ability of some Dfs to suppress toxicity may have resulted from additive effects of haplo-insufficiency for several genes within the deleted region. However, we were able to successfully refine 3 of the original 11 large deletions to two individual loci. The large Df suppressors *Df(3L)st-f13* and *Df(3L)brm11* overlapped a 43-gene region from 72C1 to 72D5. *Df(3L)ED220* further refined the area to 72C1–72D4, a 20-gene interval with mutant stocks available for 12 predicted loci (Figure S1). We tested the 12 lines and

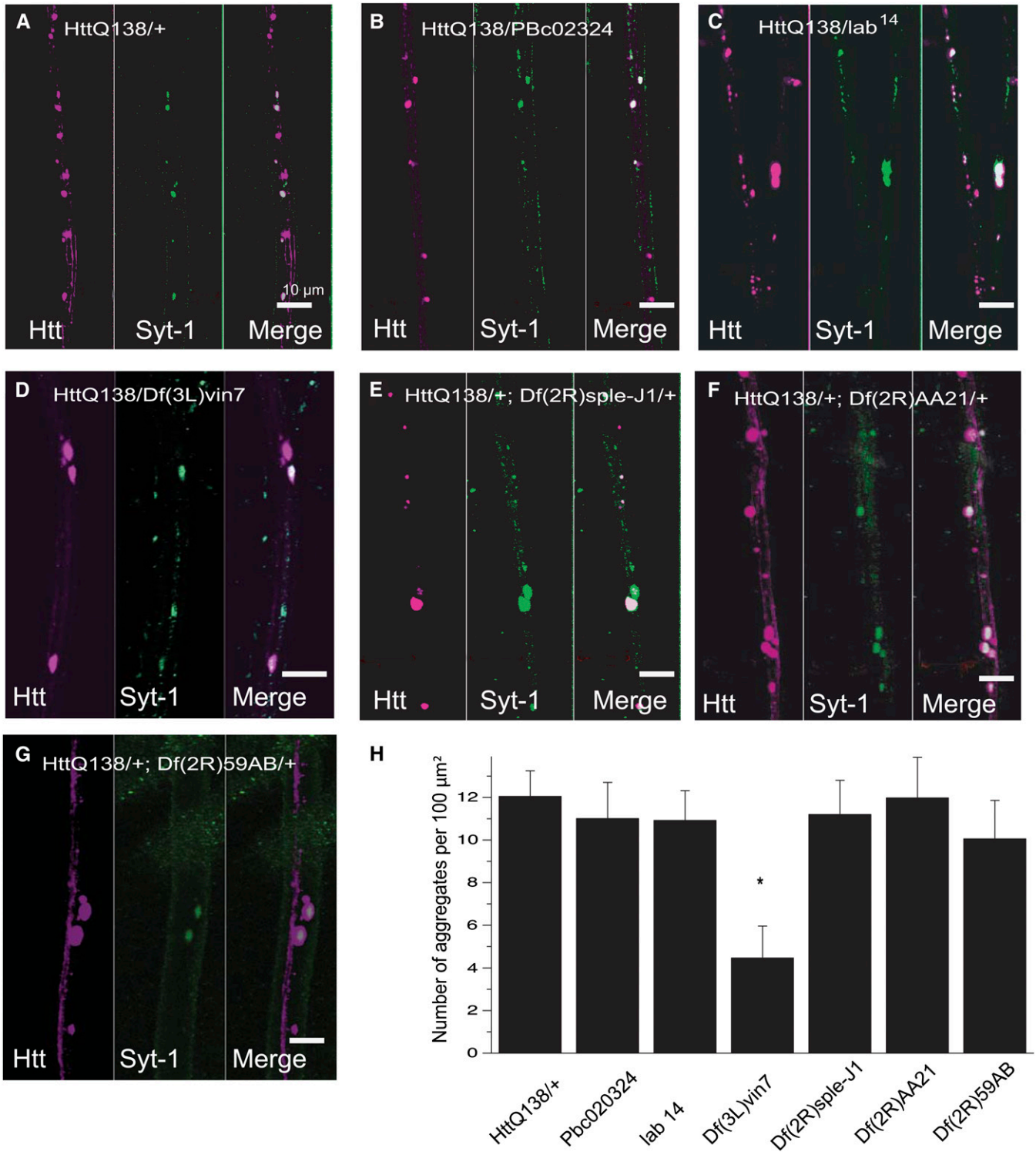

Figure 10 HttQ138 and Synaptotagmin aggregation in peripheral axons. (A–G) Confocal images of third instar larval peripheral nerves expressing mRFP-HttQ138 (magenta, left panel) and immunostained with anti-synaptotagmin I antibodies (green, center panel) from controls (A) and animals heterozygous for PBc02324 (B), *lab*^{14} (C), *Df(3L)vin7* (D), *Df(2R)sple-J1* (E), *Df(2R)AA21* (F), and *Df(2R)59AB* (G). Bars, 10 µm. (H) Quantification of HttQ138 aggregate number for 100-µm axon segments for 25 segments (n = 5 larvae) of the indicated genotypes. Aggregates >0.5 µm were counted using the "find 2D nucleus" function of the Velocity version 5.4 software (Perkin-Elmer). Error bars indicate SEM; *$P < 0.05$ using Student's t-test.

observed that stock 10887 rescued HttQ138-expressing animals at greater than the 10% expected ratio. Line 10887 (PBc02324) is a *piggyBac* transposable element insertion into the 5′ region between two genes, CG5830 and *mRpS31*. RT-PCR of line 10887 revealed that CG5830 is downregulated twofold, while *mRpS31* is not significantly affected by

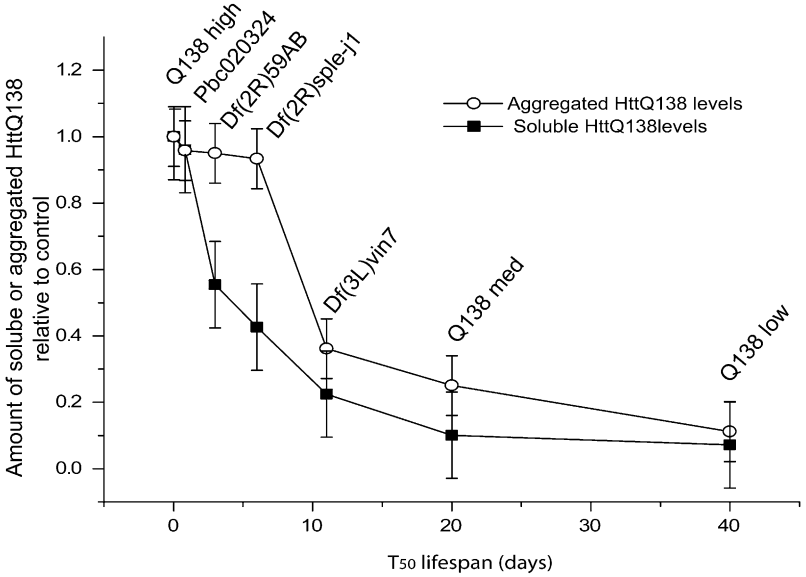

Figure 11 Graph of life span *vs.* soluble HttQ138 (measured by Western blot) or axonal aggregates (quantified per 100-μm section of larval axon) for identified suppressors. Htt expression and aggregation are tightly linked and correlate with increased toxicity. *Df(2R)sple-J1* has reduced toxicity that is correlated with decreased soluble Htt only.

the insertion (Figure S2). CG5830 is 60% identical to mammalian CTD phosphatases, which function in silencing neuronal gene expression. The repressor element 1/neuron-restrictive silencer element (REST) transcription repressor family is essential for neuronal gene silencing and has been linked to HD (Rigamonti *et al.* 2009).

The remaining interval we were able to refine to a single mutation was *Df(3R)Tpl10*, which deletes the 83C1–84B2 region and uncovers 173 genes. Screening other Dfs in this region revealed that *Df(3R)MAP117* and *Df(3R)MAP2* significantly rescued viability of HttQ138-expressing animals (Figure S1). These Dfs overlap the 84A1–84A5 interval, which contains 47 genes with 18 stocks available that disrupt loci within. We tested these strains and found that stock 2092 rescued mRFP-HttQ138–induced lethality, increasing the expected adult viability ratio to 24% *vs.* 0% in strains expressing HttQ138 alone. Stock 2092 is an X-ray–induced amorphic mutant (lab^{14}) of the *labial* gene. *Labial* is one of 8 homeobox genes in the Antennapedia cluster that play critical developmental roles in anterior–posterior body axis specification (Brody 1999). To determine whether other members of the Antennapedia HOX complex could also suppress HD pathology in our model, we tested mutations in additional members of the Antennapedia cluster for their ability to rescue HttQ138-induced lethality. Haplo-insufficiency for mutations in *Sex combs reduced* (Scr^{CP1}, 22% viability ratio; Scr^{6}, 24% viability ratio), *proboscopedia* (pr^{1}, 22% viability ratio), *Deformed* (Dfd^{6}, 15% viability ratio) and *Ultrabithorax* (Ubx^{51}, 12% viability ratio) also resulted in a significant rescue of HttQ138-induced lethality.

Both aggregated and soluble HttQ138 are likely to represent toxic species

By comparing the relative contributions of decreased aggregation and decreased soluble HttQ138 measured experimentally to increased life span, we observed a general trend whereby decreasing Htt expression causes a decrease in aggregation and an increase in viability (Figure 11). However, two suppressors uncovered in the screen displayed increased viability without a significant change in aggregation in peripheral motor axons [*Df(2R)59AB* and *Df(2R)sple-j1*]. mRFP-HttQ138 expression in these backgrounds is decreased by Western analysis and RT-PCR, but there is no change in the number of axonal aggregates (Figure 8, C and E). Additionally, *Pbc020324* and lab^{14} show increased life span without a significant change in aggregation in any cell type. These suppressor backgrounds indicate some increase in viability can be achieved independent of decreasing aggregated HttQ138. In these lines, the increase in life span is correlated with a decrease in soluble HttQ138, arguing that this form of HttQ138 may also contribute to toxicity.

Discussion

Many neurodegenerative diseases associated with protein misfolding have been modeled in *Drosophila*, including Parkinson's disease (Feany and Bender 2000), Alzheimer's disease (Wittmann *et al.* 2001), spinocerebellar ataxia type 1 (Fernandez-Funez *et al.* 2000) and type 3 (Warrick *et al.* 1999), and Huntington's disease (Jackson *et al.* 1998; Steffan *et al.* 2001; Gunawardena *et al.* 2003; Lee *et al.* 2004). These models replicate many neuropathological features characteristic of the diseases, such as late onset, progressive neurodegeneration, and formation of inclusions containing the mutant protein. Here we describe the generation of a new *Drosophila* HD model in which expression of a 588-aa N-terminal fragment of human Htt containing a 138 poly(Q) tract results in pharate adult lethality. By engineering a fluorescent tag on the mutant Htt fragment, we were able to visualize the location, trafficking, and aggregation of Htt in both neuronal and non-neuronal cells in live *Drosophila*. As such, we were able to screen independently for suppressors of Htt aggregation by following HttQ138-mRFP localization in live animals. The screens resulted in the identification of seven large Dfs

uncovering genomic regions that are capable of suppressing Htt-induced lethality without altering HttQ138 aggregate formation and four additional Dfs that suppressed both Htt-induced lethality and HttQ138 aggregation. Our findings indicate the presence of gene products downstream, or independent, of aggregation that can dominantly reduce HD toxicity. Our results also indicate that expression levels of mutant Htt are critical for disease pathology, as all Dfs we identified that reduced Htt expression levels by ~50% increased viability. As such, targeted approaches that reduce mutant Htt expression by relatively modest amounts may have profound effects on toxicity in HD patients.

The ability to follow Htt dynamics in live animals using our fluorescently tagged HttQ15 and HttQ138 trangenes revealed several important aspects of our *Drosophila* HD model. We find that both pathogenic and nonpathogenic versions of Htt are localized to the cytoplasm of all cell types examined. In humans, cleavage of Htt is thought to be important in generation of toxic Htt fragments (Qin and Gu 2004), with several studies indicating that small cleaved N-terminal fragments enter the nucleus to form intranuclear inclusions that contribute to pathogenesis (Difiglia *et al.* 1997; Sieradzan *et al.* 1999). Although evidence suggests that intranuclear aggregates can contribute to HD pathology (Davies *et al.* 1997; Becher *et al.* 1998), several studies indicate that pathogenic Htt aggregates in the cytoplasm and neurites play a causative role (Li *et al.* 1999; Sapp *et al.* 1999). As such, where toxic Htt fragments responsible for HD pathology reside in neurons remains to be conclusively identified. Using Htt fragments that were tagged at the N terminus with GFP and at the C terminus with mRFP, we demonstrate that cleavage of Htt is not apparent in *Drosophila*. In addition, expression of a smaller Htt exon 1 fragment still localizes to the cytoplasm. It is possible that addition of a GFP moiety alters Htt localization, although we observed the same pattern with an HA-tagged Htt transgenic protein as well (Lee *et al.* 2004). Thus, pathology in this HD model occurs secondary to cytoplasmic poly(Q) Htt localization.

To characterize the kinetics of Htt aggregation, we used live imaging of fluorescently tagged mRFP-HttQ138. Several studies indicate mutant Htt can disrupt FAT (Gunawardena *et al.* 2003; Szebenyi *et al.* 2003; Lee *et al.* 2004), but the mechanism by which defects occur is unclear. Since Htt is selectively toxic to neurons, an attractive model is that disrupted FAT may confer toxicity due to transport defects. Our FRAP data suggest that large immobile aggregates acquire new HttQ138 puncta. We determined the rate of FRAP recovery within aggregates was the same in both axons and the cell body, suggesting that aggregation kinetics are not solely dependent on the higher local concentrations of Htt induced by FAT. We took advantage of the Gal80^{ts} repressor to view early events in aggregate formation and visualize the aggregation progression. We observed that soluble HttQ138 forms aggregates that grow in size over a 12-hr window, decreasing the amount of soluble Htt present in the cell. Incorporation of HttQ138 into preexisting aggregates was much faster, suggesting that once aggregates are formed, they represent an active sink for accumulating new Htt protein on a minute timescale.

A key question in the HD field is whether Htt aggregates are toxic, neuroprotective, or simply by-products of the disease process. This issue is of critical importance for therapeutic considerations, as many current efforts are aimed at reducing Htt aggregation, assuming that this will decrease toxicity. Our previous observations that Htt aggregates accumulate in axons and impede axonal transport (Lee *et al.* 2004) suggested a model in which axonally localized aggregates can disrupt neuronal function. Whether aggregates in other cellular compartments cause toxicity is still an open question. The ability of drugs like Congo Red (Heiser *et al.* 2000; Sanchez *et al.* 2003), minocycline (Chen *et al.* 2000; Smith *et al.* 2003), and the transglutaminase inhibitor cystamine (Dedeoglu *et al.* 2002) to block Htt aggregation and reduce behavioral phenotypes in R6/2 Htt poly(Q) mice is suggestive of aggregate toxicity as well. Molecular (Warrick *et al.* 1999; Fernandez-Funez *et al.* 2000; Jana *et al.* 2000; Cummings *et al.* 2001; Vacher *et al.* 2005) and chemical (Yoshida *et al.* 2002) chaperones that reduce aggregate formation have been shown to reduce cytotoxicity in several poly(Q) disease models. Likewise, intracellular antibodies (Lecerf *et al.* 2001; Khoshnan *et al.* 2002; Colby *et al.* 2004; Wolfgang *et al.* 2005) that bind mutant Htt epitopes and suppress aggregate formation provide some neuroprotection in animal models. Our genetic screens support a model where aggregate formation and soluble Htt (monomers or oligomers) may both contribute to toxicity, as every Df that reduced aggregation or soluble Htt levels showed an increase in viability. The observation that we did not identify any haplo-insufficient loci capable of reducing aggregation without altering Htt expression levels suggests that aggregation inhibition alone may require more potent pharmacological effects than can be achieved with only a 50% reduction in activity of a single protein. In contrast, the finding that *Df(2R)spleJ1* and *Df(2R)59AB* increase viability without changes in aggregation suggests that HttQ138 toxicity can be reduced without altering Htt aggregation.

Although neuronal toxicity associated with Htt poly(Q) expansion has been the emphasis of most HD studies, the Htt protein is expressed in many nonneuronal tissues, including testes, liver, heart, lungs, and pancreatic islets (Ferrante *et al.* 1997; Cattaneo *et al.* 2005). HD patients have been shown to have a higher risk of diabetes (Lalic *et al.* 2008), and mouse HD models show pancreatic pathology (Martin *et al.* 2008), indicating that Htt poly(Q) expansion may also cause defects in nonneuronal cells. We found that HttQ138 expression in *Drosophila* salivary glands results in defective glue secretion (Figure 3), suggesting that nonneuronal defects from HttQ138 expression exist in our model as well. The ease with which the Sgs3-GFP glue secretion assay can be performed opens up the possibility of additional screens for second-site suppressors that alleviate salivary gland dysfunction in HttQ138-expressing animals. It

is currently unclear whether salivary cell Htt aggregates induce pathology or whether they are secondary to other defective secretion mechanisms. Htt is associated with numerous organelles, including the Golgi, the ER, clathrin-coated vesicles, synaptic vesicles, and endosomal vesicles (Velier *et al.* 1998; Hoffner *et al.* 2002; Kegel *et al.* 2002). In addition, Htt interacts with numerous vesicle-trafficking proteins, including dynamin, huntingtin-interacting protein 1 (HIP1), and huntingtin-associated protein1 (HAP1), which binds the p150glued subunit of dynactin (Li *et al.* 1998). Potential defects in vesicle trafficking or fusion may thus account for the defects observed in glue secretion.

The results from our haplo-insufficiency screen provide several clues regarding the role of soluble and aggregated forms of Htt and their contribution to toxicity, but no clear information about cellular pathways disrupted by HD. We mapped the suppression mediated by three large Dfs down to two single genes. One of our hits was a *piggyBac* insertion in strain PBc020324 in the small 5′ interval between CG5830 and *mRpS3*, which reduces CG5830 expression. CG5830 encodes a phosphatase with sequence homology to small CTD phosphatases that function in silencing neuronal gene expression (Yeo *et al.* 2005). Disruption of neurotrophic factor expression, especially BDNF through aberrant function of its transcriptional repressor REST/NRSF, has been implicated in HD mouse models and in cortex of patients with HD (Zuccato *et al.* 2001, 2003; Buckley *et al.* 2010). It will be important to test whether previously identified *Drosophila* neurotrophic proteins (Zhu *et al.* 2008) are dysregulated in mRFP-HttQ138–expressing animals and whether haplo-insufficiency of CG5830 reduces this effect. Although Pbc020324 is likely rescuing toxicity in part by reducing Htt transgene expression, we did not observe any decrease in HttQ138 aggregation or protein levels by Western analysis. This discrepancy between reduced transcription and Htt protein levels and aggregation suggests CG5830 may have other neuroprotective effects as well.

The other single gene we mapped, *Labial* is a member of the ANTP complex and has been linked to neural stem cell survival during postembryonic neurogenesis in *Drosophila* (Bello *et al.* 2007). Mutant Htt has been implicated in transcriptional dysregulation of a broad range of genes, reducing levels of highly pleiotropic proteins like RNA polymerase II (Luthi-Carter *et al.* 2002) and facilitating expression in mice of polycomb repressive complex 2, which specifically regulates HOX gene expression (Seong *et al.* 2010). Htt has also been linked to HOX gene regulation through the poly(Q) and poly-Proline regions shared between Htt and several transcriptional regulators, including *Sex combs reduced* (Gerber *et al.* 1994). Similar to Pbc020324, this mutation decreases Htt transgene transcription, but has no effect on aggregation. The decreased Htt transcription in the *hox* mutants likely contributes to the suppressive effects of these strains. However, an additional effect suggested by microarray analysis of Htt-poly(Q)–expressing brains in *Drosophila* (W. C.-M. Lee and J. T. Littleton, unpublished data) is that ANTP genes are upregulated in HD and contribute to neuropathology. Several Hox genes, including *labial*, *proboscipedia*, and *Sex combs reduced*, were increased in Htt-poly (Q) brains, suggesting that haplo-insufficiency for these loci might function to reduce Htt expression to a less toxic level. Further studies will be needed to dissect this link between the homeotic genes and HD pathology.

Examining the pattern by which suppressor mutations interact with HttQ138 provides insight into the role of aggregates in toxicity. The weakest suppressors had no alteration in aggregation or HttQ138 expression, suggesting some minor rescue is possible without disrupting aggregation. A larger increase in viability occurs with decreased expression of HttQ138, but little to no change in aggregated Htt, suggesting that soluble HttQ138 is a toxic species in these cases. The final group of suppressors increased viability even more, while decreasing both soluble and aggregated Htt. In summary, we have generated a new HD model in *Drosophila* that allows for *in vivo* analysis of pathogenic Htt localization, aggregation, and dynamics. Using this model, we identified several genetic suppressors that can reduce HttQ138-mediated toxicity. The most robust suppressors reduced both soluble and aggregated Htt levels, suggesting that toxicity is likely to be associated with both forms of the mutant protein.

Acknowledgments

We thank David Housman for kindly providing the HttQ96-GFP construct; Katie Lynch for help with subcloning the HttQ96-GFP construct; Albert Su, Grace Lin, and Rupali Avasare for S2 cell experiments; Andrew Andres for providing the Sgs3-GFP–expressing *Drosophila*; and Ray Truant for HttQ15 and HttQ138 cDNAs.

Literature Cited

Arrasate, M., S. Mitra, E. S. Schweitzer, M. R. Segal, and S. Finkbeiner, 2004 Inclusion body formation reduces levels of mutant huntingtin and the risk of neuronal death. Nature 431: 805–810.

Becher, M. W., J. A. Kotzuk, A. H. Sharp, S. W. Davies, G. P. Bates *et al.*, 1998 Intranuclear neuronal inclusions in Huntington's disease and dentatorubral and pallidoluysian atrophy: correlation between the density of inclusions and IT15 CAG triplet repeat length. Neurobiol. Dis. 4: 387–397.

Bello, B., N. Holbro, and H. Reichert, 2007 Polycomb group genes are required for neural stem cell survival in postembryonic neurogenesis of Drosophila. Development 134: 1091–1099.

Biyasheva, A., T. V. Do, Y. Lu, M. Vaskova, and A. J. Andres, 2001 Glue secretion in the Drosophila salivary gland: a model for steroid-regulated exocytosis. Dev. Biol. 231: 234–251.

Brody, T., 1999 The interactive fly: gene networks, development and the Internet. Trends Genet. 15: 333–334.

Buckley, N. J., R. Johnson, C. Zuccato, A. Bithell, and E. Cattaneo, 2010 The role of REST in transcriptional and epigenetic dysregulation in Huntington's disease. Neurobiol. Dis. 39: 28–39.

Campbell, R. E., O. Tour, A. E. Palmer, P. A. Steinbach, G. S. Baird *et al.*, 2002 A monomeric red fluorescent protein. Proc. Natl. Acad. Sci. USA 99: 7877–7882.

Carmichael, J., J. Chatellier, A. Woolfson, C. Milstein, A. R. Fersht *et al.*, 2000 Bacterial and yeast chaperones reduce both aggregate formation and cell death in mammalian cell models of Huntington's disease. Proc. Natl. Acad. Sci. USA 97: 9701–9705.

Cattaneo, E., C. Zuccato, and M. Tartari, 2005 Normal huntingtin function: an alternative approach to Huntington's disease. Nat. Rev. Neurosci. 6: 919–930.

Chai, Y., J. Shao, V. M. Miller, A. Williams, and H. L. Paulson, 2002 Live-cell imaging reveals divergent intracellular dynamics of polyglutamine disease proteins and supports a sequestration model of pathogenesis. Proc. Natl. Acad. Sci. USA 99: 9310–9315.

Chen, M., V. O. Ona, M. Li, R. J. Ferrante, K. B. Fink *et al.*, 2000 Minocycline inhibits caspase-1 and caspase-3 expression and delays mortality in a transgenic mouse model of Huntington disease. Nat. Med. 6: 797–801.

Chopra, V., J. H. Fox, G. Lieberman, K. Dorsey, W. Matson *et al.*, 2007 A small-molecule therapeutic lead for Huntington's disease: preclinical pharmacology and efficacy of C2–8 in the R6/2 transgenic mouse. Proc. Natl. Acad. Sci. USA 104: 16685–16689.

Colby, D. W., Y. Chu, J. P. Cassady, M. Duennwald, H. Zazulak *et al.*, 2004 Potent inhibition of huntingtin aggregation and cytotoxicity by a disulfide bond-free single-domain intracellular antibody. Proc. Natl. Acad. Sci. USA 101: 17616–17621.

Cummings, C. J., Y. Sun, P. Opal, B. Antalffy, R. Mestril *et al.*, 2001 Over-expression of inducible HSP70 chaperone suppresses neuropathology and improves motor function in SCA1 mice. Hum. Mol. Genet. 10: 1511–1518.

Davies, S. W., M. Turmaine, B. A. Cozens, M. DiFiglia, A. H. Sharp *et al.*, 1997 Formation of neuronal intranuclear inclusions underlies the neurological dysfunction in mice transgenic for the HD mutation. Cell 90: 537–548.

Dedeoglu, A., J. K. Kubilus, T. M. Jeitner, S. A. Matson, M. Bogdanov *et al.*, 2002 Therapeutic effects of cystamine in a murine model of Huntington's disease. J. Neurosci. 22: 8942–8950.

DiFiglia, M., E. Sapp, K. O. Chase, S. W. Davies, G. P. Bates *et al.*, 1997 Aggregation of huntingtin in neuronal intranuclear inclusions and dystrophic neurites in brain. Science 277: 1990–1993.

Feany, M. B., and W. W. Bender, 2000 A Drosophila model of Parkinson's disease. Nature 404: 394–398.

Fernandez-Funez, P., M. L. Nino-Rosales, B. de Gouyon, W. C. She, J. M. Luchak *et al.*, 2000 Identification of genes that modify ataxin-1-induced neurodegeneration. Nature 408: 101–106.

Ferrante, R. J., C. A. Gutekunst, F. Persichetti, S. M. McNeil, N. W. Kowall *et al.*, 1997 Heterogeneous topographic and cellular distribution of huntingtin expression in the normal human neostriatum. J. Neurosci. 17: 3052–3063.

Fuger, P., L. B. Behrends, S. Mertel, S. J. Sigrist, and T. M. Rasse, 2007 Live imaging of synapse development and measuring protein dynamics using two-color fluorescence recovery after photo-bleaching at Drosophila synapses. Nat. Protoc. 2: 3285–3298.

Gafni, J., E. Hermel, J. E. Young, C. L. Wellington, M. R. Hayden *et al.*, 2004 Inhibition of calpain cleavage of huntingtin reduces toxicity: accumulation of calpain/caspase fragments in the nucleus. J. Biol. Chem. 279: 20211–20220.

Gerber, H. P., K. Seipel, O. Georgiev, M. Hofferer, M. Hug *et al.*, 1994 Transcriptional activation modulated by homopolymeric glutamine and proline stretches. Science 263: 808–811.

Graham, R. K., Y. Deng, E. J. Slow, B. Haigh, N. Bissada *et al.*, 2006 Cleavage at the caspase-6 site is required for neuronal dysfunction and degeneration due to mutant huntingtin. Cell 125: 1179–1191.

Gunawardena, S., L. S. Her, R. G. Brusch, R. A. Laymon, I. R. Niesman *et al.*, 2003 Disruption of axonal transport by loss of huntingtin or expression of pathogenic polyQ proteins in Drosophila. Neuron 40: 25–40.

Harjes, P., and E. E. Wanker, 2003 The hunt for huntingtin function: interaction partners tell many different stories. Trends Biochem. Sci. 28: 425–433.

Heiser, V., E. Scherzinger, A. Boeddrich, E. Nordhoff, R. Lurz *et al.*, 2000 Inhibition of huntingtin fibrillogenesis by specific antibodies and small molecules: implications for Huntington's disease therapy. Proc. Natl. Acad. Sci. USA 97: 6739–6744.

Hodgson, J. G., N. Agopyan, C. A. Gutekunst, B. R. Leavitt, F. LePiane *et al.*, 1999 A YAC mouse model for Huntington's disease with full-length mutant huntingtin, cytoplasmic toxicity, and selective striatal neurodegeneration. Neuron 23: 181–192.

Hoffner, G., P. Kahlem, and P. Djian, 2002 Perinuclear localization of huntingtin as a consequence of its binding to microtubules through an interaction with beta-tubulin: relevance to Huntington's disease. J. Cell Sci. 115: 941–948.

Hoffner, G., M. L. Island, and P. Djian, 2005 Purification of neuronal inclusions of patients with Huntington's disease reveals a broad range of N-terminal fragments of expanded huntingtin and insoluble polymers. J. Neurochem. 95: 125–136.

Huntington's Disease Research Collaboration, 1993 A novel gene containing a trinucleotide repeat that is expanded and unstable on Huntington's disease chromosomes. Cell. 72: 971–983.

Jackson, G. R., I. Salecker, X. Dong, X. Yao, N. Arnheim *et al.*, 1998 Polyglutamine-expanded human huntingtin transgenes induce degeneration of Drosophila photoreceptor neurons. Neuron 21: 633–642.

Jana, N. R., M. Tanaka, G. Wang, and N. Nukina, 2000 Polyglutamine length-dependent interaction of Hsp40 and Hsp70 family chaperones with truncated N-terminal huntingtin: their role in suppression of aggregation and cellular toxicity. Hum. Mol. Genet. 9: 2009–2018.

Kegel, K. B., A. R. Meloni, Y. Yi, Y. J. Kim, E. Doyle *et al.*, 2002 Huntingtin is present in the nucleus, interacts with the transcriptional corepressor C-terminal binding protein, and represses transcription. J. Biol. Chem. 277: 7466–7476.

Khoshnan, A., J. Ko, and P. H. Patterson, 2002 Effects of intracellular expression of anti-huntingtin antibodies of various specificities on mutant huntingtin aggregation and toxicity. Proc. Natl. Acad. Sci. USA 99: 1002–1007.

Kim, Y. J., Y. Yi, E. Sapp, Y. Wang, B. Cuiffo *et al.*, 2001 Caspase 3-cleaved N-terminal fragments of wild-type and mutant huntingtin are present in normal and Huntington's disease brains, associate with membranes, and undergo calpain-dependent proteolysis. Proc. Natl. Acad. Sci. USA 98: 12784–12789.

Kimura, Y., W. C. Lee, and J. T. Littleton, 2007 Therapeutic prospects for the prevention of neurodegeneration in Huntington's disease and the polyglutamine repeat disorders. Mini Rev. Med. Chem. 7: 99–106.

Krobitsch, S., and S. Lindquist, 2000 Aggregation of huntingtin in yeast varies with the length of the polyglutamine expansion and the expression of chaperone proteins. Proc. Natl. Acad. Sci. USA 97: 1589–1594.

Kuemmerle, S., C. A. Gutekunst, A. M. Klein, X. J. Li, S. H. Li *et al.*, 1999 Huntington aggregates may not predict neuronal death in Huntington's disease. Ann. Neurol. 46: 842–849.

Lajoie, P., and E. L. Snapp, 2010 Formation and toxicity of soluble polyglutamine oligomers in living cells. PLoS ONE 5: e15245.

Lalic, N. M., J. Maric, M. Svetel, A. Jotic, E. Stefanova *et al.*, 2008 Glucose homeostasis in Huntington disease: abnormalities in insulin sensitivity and early-phase insulin secretion. Arch. Neurol. 65: 476–480.

Lam, W., W. M. Chan, T. W. Lo, A. K. Wong, C. C. Wu *et al.*, 2008 Human receptor for activated protein kinase C1 associ-

ates with polyglutamine aggregates and modulates polyglutamine toxicity. Biochem. Biophys. Res. Commun. 377: 714–719.
Lecerf, J. M., T. L. Shirley, Q. Zhu, A. Kazantsev, P. Amersdorfer *et al.*, 2001 Human single-chain Fv intrabodies counteract in situ huntingtin aggregation in cellular models of Huntington's disease. Proc. Natl. Acad. Sci. USA 98: 4764–4769.
Lee, W. C., M. Yoshihara, and J. T. Littleton, 2004 Cytoplasmic aggregates trap polyglutamine-containing proteins and block axonal transport in a Drosophila model of Huntington's disease. Proc. Natl. Acad. Sci. USA 101: 3224–3229.
Li, H., S. H. Li, A. L. Cheng, L. Mangiarini, G. P. Bates *et al.*, 1999 Ultrastructural localization and progressive formation of neuropil aggregates in Huntington's disease transgenic mice. Hum. Mol. Genet. 8: 1227–1236.
Li, H., S. H. Li, Z. X. Yu, P. Shelbourne, and X. J. Li, 2001 Huntingtin aggregate-associated axonal degeneration is an early pathological event in Huntington's disease mice. J. Neurosci. 21: 8473–8481.
Li, S. H., C. A. Gutekunst, S. M. Hersch, and X. J. Li, 1998 Interaction of huntingtin-associated protein with dynactin P150Glued. J. Neurosci. 18: 1261–1269.
Lunkes, A., K. S. Lindenberg, L. Ben-Haiem, C. Weber, D. Devys *et al.*, 2002 Proteases acting on mutant huntingtin generate cleaved products that differentially build up cytoplasmic and nuclear inclusions. Mol. Cell 10: 259–269.
Luthi-Carter, R., S. A. Hanson, A. D. Strand, D. A. Bergstrom, W. Chun *et al.*, 2002 Dysregulation of gene expression in the R6/2 model of polyglutamine disease: parallel changes in muscle and brain. Hum. Mol. Genet. 11: 1911–1926.
Martin, B., E. Golden, A. Keselman, M. Stone, M. P. Mattson *et al.*, 2008 Therapeutic perspectives for the treatment of Huntington's disease: treating the whole body. Histol. Histopathol. 23: 237–250.
Nagai, Y., T. Inui, H. A. Popiel, N. Fujikake, K. Hasegawa *et al.*, 2007 A toxic monomeric conformer of the polyglutamine protein. Nat. Struct. Mol. Biol. 14: 332–340.
Orr, H. T., and H. Y. Zoghbi, 2007 Trinucleotide repeat disorders. Annu. Rev. Neurosci. 30: 575–621.
Park, J. H., A. J. Schroeder, C. Helfrich-Forster, F. R. Jackson, and J. Ewer, 2003 Targeted ablation of CCAP neuropeptide-containing neurons of Drosophila causes specific defects in execution and circadian timing of ecdysis behavior. Development 130: 2645–2656.
Persichetti, F., F. Trettel, C. C. Huang, C. Fraefel, H. T. Timmers *et al.*, 1999 Mutant huntingtin forms in vivo complexes with distinct context-dependent conformations of the polyglutamine segment. Neurobiol. Dis. 6: 364–375.
Portera-Cailliau, C., J. C. Hedreen, D. L. Price, and V. E. Koliatsos, 1995 Evidence for apoptotic cell death in Huntington disease and excitotoxic animal models. J. Neurosci. 15: 3775–3787.
Qin, Z. H., and Z. L. Gu, 2004 Huntingtin processing in pathogenesis of Huntington disease. Acta Pharmacol. Sin. 25: 1243–1249.
Rieckhof, G. E., M. Yoshihara, Z. Guan, and J. T. Littleton, 2003 Presynaptic N-type calcium channels regulate synaptic growth. J. Biol. Chem. 278: 41099–41108.
Rigamonti, D., C. Mutti, C. Zuccato, E. Cattaneo, and A. Contini, 2009 Turning REST/NRSF dysfunction in Huntington's disease into a pharmaceutical target. Curr. Pharm. Des. 15: 3958–3967.
Romero, E., G. H. Cha, P. Verstreken, C. V. Ly, R. E. Hughes *et al.*, 2008 Suppression of neurodegeneration and increased neurotransmission caused by expanded full-length huntingtin accumulating in the cytoplasm. Neuron 57: 27–40.
Sanchez, I., C. Mahlke, and J. Yuan, 2003 Pivotal role of oligomerization in expanded polyglutamine neurodegenerative disorders. Nature 421: 373–379.
Sapp, E., J. Penney, A. Young, N. Aronin, J. P. Vonsattel *et al.*, 1999 Axonal transport of N-terminal huntingtin suggests early pathology of corticostriatal projections in Huntington disease. J. Neuropathol. Exp. Neurol. 58: 165–173.
Scherzinger, E., R. Lurz, M. Turmaine, L. Mangiarini, B. Hollenbach *et al.*, 1997 Huntingtin-encoded polyglutamine expansions form amyloid-like protein aggregates in vitro and in vivo. Cell 90: 549–558.
Scherzinger, E., A. Sittler, K. Schweiger, V. Heiser, R. Lurz *et al.*, 1999 Self-assembly of polyglutamine-containing huntingtin fragments into amyloid-like fibrils: implications for Huntington's disease pathology. Proc. Natl. Acad. Sci. USA 96: 4604–4609.
Seong, I. S., J. M. Woda, J. J. Song, A. Lloret, P. D. Abeyrathne *et al.*, 2010 Huntingtin facilitates polycomb repressive complex 2. Hum. Mol. Genet. 19: 573–583.
Sieradzan, K. A., A. O. Mechan, L. Jones, E. E. Wanker, N. Nukina *et al.*, 1999 Huntington's disease intranuclear inclusions contain truncated, ubiquitinated huntingtin protein. Exp. Neurol. 156: 92–99.
Sinadinos, C., T. Burbidge-King, D. Soh, L. M. Thompson, J. L. Marsh *et al.*, 2009 Live axonal transport disruption by mutant huntingtin fragments in Drosophila motor neuron axons. Neurobiol. Dis. 34: 389–395.
Slow, E. J., R. K. Graham, A. P. Osmand, R. S. Devon, G. Lu *et al.*, 2005 Absence of behavioral abnormalities and neurodegeneration in vivo despite widespread neuronal huntingtin inclusions. Proc. Natl. Acad. Sci. USA 102: 11402–11407.
Smith, D. L., B. Woodman, A. Mahal, K. Sathasivam, S. Ghazi-Noori *et al.*, 2003 Minocycline and doxycycline are not beneficial in a model of Huntington's disease. Ann. Neurol. 54: 186–196.
Steffan, J. S., L. Bodai, J. Pallos, M. Poelman, A. McCampbell *et al.*, 2001 Histone deacetylase inhibitors arrest polyglutamine-dependent neurodegeneration in Drosophila. Nature 413: 739–743.
Szebenyi, G., G. A. Morfini, A. Babcock, M. Gould, K. Selkoe *et al.*, 2003 Neuropathogenic forms of huntingtin and androgen receptor inhibit fast axonal transport. Neuron 40: 41–52.
Tagawa, K., M. Hoshino, T. Okuda, H. Ueda, H. Hayashi *et al.*, 2004 Distinct aggregation and cell death patterns among different types of primary neurons induced by mutant huntingtin protein. J. Neurochem. 89: 974–987.
Vacher, C., L. Garcia-Oroz, and D. C. Rubinsztein, 2005 Overexpression of yeast hsp104 reduces polyglutamine aggregation and prolongs survival of a transgenic mouse model of Huntington's disease. Hum. Mol. Genet. 14: 3425–3433.
Velier, J., M. Kim, C. Schwarz, T. W. Kim, E. Sapp *et al.*, 1998 Wild-type and mutant huntingtins function in vesicle trafficking in the secretory and endocytic pathways. Exp. Neurol. 152: 34–40.
Vomel, M., and C. Wegener, 2007 Neurotransmitter-induced changes in the intracellular calcium concentration suggest a differential central modulation of CCAP neuron subsets in Drosophila. Dev. Neurobiol. 67: 792–808.
Vonsattel, J. P., R. H. Myers, T. J. Stevens, R. J. Ferrante, E. D. Bird *et al.*, 1985 Neuropathological classification of Huntington's disease. J. Neuropathol. Exp. Neurol. 44: 559–577.
Warrick, J. M., H. Y. Chan, G. L. Gray-Board, Y. Chai, H. L. Paulson *et al.*, 1999 Suppression of polyglutamine-mediated neurodegeneration in Drosophila by the molecular chaperone HSP70. Nat. Genet. 23: 425–428.
Wellington, C. L., L. M. Ellerby, C. A. Gutekunst, D. Rogers, S. Warby *et al.*, 2002 Caspase cleavage of mutant huntingtin precedes neurodegeneration in Huntington's disease. J. Neurosci. 22: 7862–7872.
Wittmann, C. W., M. F. Wszolek, J. M. Shulman, P. M. Salvaterra, J. Lewis *et al.*, 2001 Tauopathy in Drosophila: neurodegeneration without neurofibrillary tangles. Science 293: 711–714.

Wolfgang, W. J., T. W. Miller, J. M. Webster, J. S. Huston, L. M. Thompson *et al.*, 2005 Suppression of Huntington's disease pathology in Drosophila by human single-chain Fv antibodies. Proc. Natl. Acad. Sci. USA 102: 11563–11568.

Yeo, M., S. K. Lee, B. Lee, E. C. Ruiz, S. L. Pfaff *et al.*, 2005 Small CTD phosphatases function in silencing neuronal gene expression. Science 307: 596–600.

Yoshida, H., T. Yoshizawa, F. Shibasaki, S. Shoji, and I. Kanazawa, 2002 Chemical chaperones reduce aggregate formation and cell death caused by the truncated Machado-Joseph disease gene product with an expanded polyglutamine stretch. Neurobiol. Dis. 10: 88–99.

Zhu, B., J. A. Pennack, P. McQuilton, M. G. Forero, K. Mizuguchi *et al.*, 2008 Drosophila neurotrophins reveal a common mechanism for nervous system formation. PLoS Biol. 6: e284.

Zuccato, C., A. Ciammola, D. Rigamonti, B. R. Leavitt, D. Goffredo *et al.*, 2001 Loss of huntingtin-mediated BDNF gene transcription in Huntington's disease. Science 293: 493–498.

Zuccato, C., M. Tartari, A. Crotti, D. Goffredo, M. Valenza *et al.*, 2003 Huntingtin interacts with REST/NRSF to modulate the transcription of NRSE-controlled neuronal genes. Nat. Genet. 35: 76–83.

Communicating editor: T. R. Magnuson

GENETICS

Supporting Information
http://www.genetics.org/content/suppl/2011/11/17/genetics.111.133710.DC1

Huntingtin Aggregation Kinetics and Their Pathological Role in a *Drosophila* Huntington's Disease Model

Kurt R. Weiss, Yoko Kimura, Wyan-Ching Mimi Lee, and J. Troy Littleton

DOI: 10.1534/genetics.111.133710

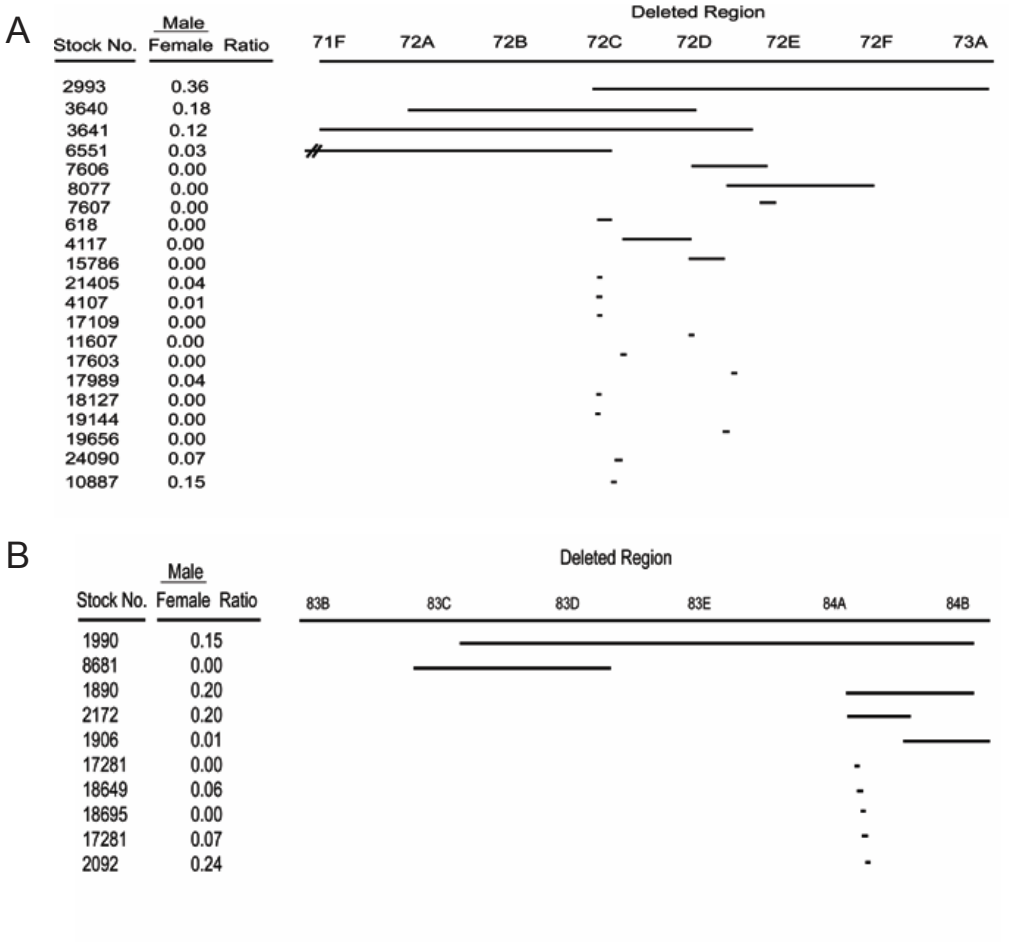

Figure S1 Fine mapping for two genetic intervals uncovered in the initial suppressor screen for HttQ138 pupal lethality. (A) Suppressors *Df(3L)st-f13* (Bloomington stock 2993) and *Df(3L)brm11* (Bloomington stock 3640) overlap the 72C1-72D5 interval. Mapping with additional aberrations contained within the Bloomington Stock Center demonstrated that stock 10887 (PBc02324) rescued HttQ138 expressing animals at 15% of expected viability. (B) Suppressor *Df(3R)Tpl10* (Bloomington stock 1990) was sub-mapped to a single genetic aberration within the region defined by stock 2092 (lab^{14}) that increased the expected adult viability ratio to 24%.

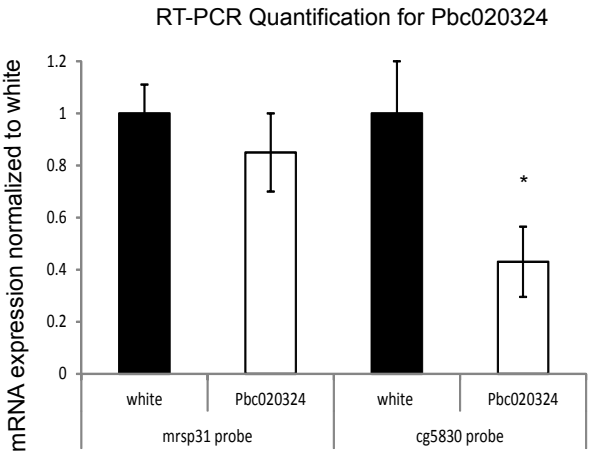

Figure S2 Quantitative RT-PCR was performed on the PBc02324 p-element insertion mutant. The transcript levels of both genes surrounding the insertion, CG5830 and *mRpS31*, were measured in homozygous mutant heads compared to white flies. Both genes appear slightly downregulated in the mutant, but only CG5830 was statistically significant. Error bars indicate SEM, with * denoting $p<0.05$ using Student's t-test.

File S1

Time-lapse confocal images of *CCAP*-GAL4; mRFP-HttQ138 showing FRAP of four aggregates of various sizes.

Frame rate is 1 per 60 seconds for a total time of 60 minutes.

File S1 is available for download at as a movie file.

Table S1 Table showing the 166 Bloomington deficiency kit strains that were tested in the initial screen, along with the number of viable flies and changes in salivary gland aggregation. The viability data is represented graphically in figure 8A.

Table S2 Table showing stocks used for mapping of screen hits. Control data is listed on the first page. Each additional page heading represents mapping from the original large Df identified in the screen. The cells within each page list most of the smaller deficiencies tested in each region and their results for viability and/or aggregation where applicable.

Tables S1 and S2 are available for download at as excel files.